UTRECHT UNIVERSITY

PV performance during low irradiance and rainy weather conditions

Master thesis Energy Science

K.B.D. Esmeijer

4/17/2014

Supervisors: A. Louwen, W.G.J.H.M. van Sark
2nd reader: B. Elsinga

Abstract

With data made available by a photovoltaic (PV) test facility located on top of an office building of the Utrecht University the performance of ten PV modules during time periods of low irradiance and precipitation was analysed. Using values for direct irradiance by Bird's SPCTRAL2 model and measured climatic conditions a weather classification system was designed in order to categorize time periods and make a comparison between rainy and non-rainy time periods possible. Results show that precipitation induces a blue shift in the solar spectrum increasing the short-circuit current (I_{SC}) of the modules (a-Si and CdTe in particular). Furthermore it is shown that precipitation causes module temperature to drop resulting in an increase in open-circuit voltage (V_{OC}) for all modules. In terms of the performance ratio (PR) it is shown that almost all modules perform better under rainy than under non-rainy weather conditions, but it is noted that incorrect measurements of module temperature most likely overestimate the PR for some of the investigated modules.

Acknowledgements

First of all I would like to thank Atse Louwen for his open door policy and allowing me to ask for guidance at any moment he was at the office. Being able to spar about which direction to take in my research and helping me with the wonderful world of Wolfram Mathematica really helped me in getting the results which I hoped for. Secondly I would like to thank Boudewijn Elsinga for his critical inputs on the irradiance model and Arjen de Waal with his knowledge about the test facility. Also I would like to thank Boudewijn Pannebakker who was always open for discussion and with whom I shared my love for debugging. Without the unlimited access to your free coffee card I don't think either of us would have seen our project through to the end. Finally I would like to thank Wilfried van Sark for giving me the opportunity to perform this research in the PV-group in the first place and allowing me to acquire skills in drafting academic papers through the work I performed under his supervision for the faculty.

1 Introduction

1.1 Justification

The performance of photovoltaic (PV) modules is generally measured indoors under standard test conditions (STC) of 25 °C module temperature and an AM1.5 broadband irradiance of 1000 Wm^{-2}. Under outdoor weather conditions this standard is however rarely met. Under cloudy weather conditions for instance the spectrum of downwelling irradiance differs from that under clear sky conditions [1]. In the Netherlands there are few hours a year in which there are no clouds present. Furthermore time periods in which precipitation is measured are also not uncommon in the Netherlands [2]. In recent years more and more research has been conducted towards ascertaining the outdoor performance of PV systems. The classification systems used to differentiate between certain weather conditions differed for most of these studies.
The growing share of a-Si based PV modules for instance has already seen an increase in research focussed on the solar spectral effects on PV system performance. Studies performed at several outdoor test facilities have made use of various methods in their selection and classification of data. Fine weather conditions for instance were classified by irradiances of more than 850 and 750 Wm^{-2} in two different studies performed by the National Institute of Advanced Industrial Science and Technology (AIST) in Japan [3, 4]. In yet another study performed by AIST, where a distinction in weather types was made, irradiances exceeding 600 Wm^{-2} were assumed to be related to fine weather conditions and those in the range of 100 - 400 Wm^{-2} to cloudy weather conditions [5]. Nofuentes et al. also attributed irradiances exceeding 600 Wm^{-2} to fine weather conditions but chose a different range of 300 – 600 W m^{-2} for cloudy weather in Spain [6]. Cornaro and Andreotti, instead of using fine and cloudy weather data, differentiate between clear and overcast conditions for Italy [7] based on the sky condition classification used by Rahim et al. [8]. Sutterlueti et al., in Switzerland and Arizona, distinguish between yet other weather types (*Clear morning*, *Clear noon*, *Diffuse sky*, *Clear evening* and *Other*) which they classified according to the global irradiance, clearness index and time of day [9]. Usami and Kawasaki use a so called “revised clearness index” for their classification and included diffuse spectra of rainy skies to their analyses in Japan [10]. Their research however did not focus on linking different weather spectra to PV module performance.

1.2 Research question

From the reviewed literature it can be derived that there is ambiguity in the methods applied to determine irradiance and weather profiles. Subsequently a comparison of “cloudy” weather results obtained from different test facilities becomes difficult. Furthermore research focussed on identifying the performance of PV modules specifically in rainy weather conditions is, to our knowledge, non-existent. In light of this gap in knowledge the research question is formulated as follows:

What is the performance of PV modules under low irradiance and rainy weather conditions?

The effects of precipitation are determined by comparing performance under low irradiance and rain with those under low irradiance and no rain. Differences in physical module properties and climatic conditions during both weather conditions are analysed in order to identify possible

drivers for performance enhancement/impedance. The main research question can therefore be subdivided into two following two:

What is the effect of precipitation on physical module properties and climatic conditions?

How is the performance of PV modules affected by precipitation induced changes in climatic conditions and physical module properties?

Indices of cloud cover identification used in previous studies are combined with irradiance and precipitation measurements in order to make a novel weather classification system. This system is used to distinguish between certain weather conditions and serves as a tool to select and group data to be analysed. The data used in this work is made available by the Utrecht Photovoltaic Outdoor Test facility (UPOT) which collects performance data of several PV modules spanning the full range of today's commercially available PV modules as well as weather data [11].

1.3 Outline

A short review of the theory behind the concepts addressed in later sections will be given in section 2. Section 3 will give a description of the experimental setup which has been used for this work and give insights into the methods applied. An overview of the results will be shown in section 4 and section 5 will address some points of discussion and indicate recommendations for possible future research. Section 6 finally will present the conclusion of this work.

2 Theoretic framework

2.1 Solar radiation

2.1.1 Solar spectral irradiance

Solar radiation of photons, as described by the wave-particle duality theory, can be considered as resonating at wavelength λ (in m) and having energy $E_{photon}(\lambda)$ (in J):

$$E_{photon}(\lambda) = \frac{h * c}{\lambda} = h * \nu$$

Equation 1

Here, h is Planck's constant ($6.62*10^{-34}$ m^2kg/s), c is the speed of light ($2.99*10^8$ m/s) and ν is the wavelength frequency (in m^{-1}). Given that h and c are constants it becomes clear from Equation 1 that high energy photons have a short wavelength and vice versa. The number of photons at a certain wavelength that fall per second on a square meter is given by the *Photon Flux Density* $\Phi(\lambda)$:

$$\Phi(\lambda) = \frac{\#\ of\ photons\ (\lambda)}{s * m^2}$$

Equation 2

The product of $E_{photon}(\lambda)$ and $\Phi(\lambda)$ at a certain wavelength that fall on one square meter per second is what is known as the *Spectral Irradiance* $E_\lambda(\lambda)$:

$$E_\lambda(\lambda) = E_{photon}(\lambda) * \Phi(\lambda)$$

Equation 3

Integration of the spectral irradiance over a wavelength range gives rise to the *Total Irradiance G* (or *Broadband Irradiance* in W/m^2) [12]:

$$G = \int E_\lambda(\lambda) d\lambda$$

Equation 4

2.1.2 Total irradiance on earth's surface

Not all photons present in the extra-terrestrial radiation reaching the earth's outer atmosphere will contribute to *G*. Apart from some of the radiation being reflected back into space, several transmittance functions need to be taken into consideration which account for scattering and absorption of photons by particles in the atmosphere. The actual composition of *G* reaching the earth's surface has been estimated by several models over the years. One of these, the SPCTRAL2 model as proposed by Bird, uses wavelength dependent functions to estimate *G* [13]. They pertain to molecular Rayleigh scattering, aerosol attenuation, water vapour absorption, ozone absorption and uniformly mixed gas absorption. This model will be discussed more elaborately in section 3.5.1 . For now it will suffice to mention that accounting for the aforementioned transmittance functions will give an accurate estimation of the broadband irradiance which reaches the earth's surface.

2.1.3 Direct and diffuse irradiance

A distinction can be made between the solar radiation which is observable directly from the sun's disc (direct irradiance or I_{direct}) and that which is scattered by cloud and dust particles in all directions (diffuse irradiance or $I_{diffuse}$). Figure 1 shows the origin of these irradiances. It must be noted that the ratio between direct and diffuse irradiance differs as skies change from clear to overcast. On clear skies there is always at least 10% diffuse irradiance measurable, whereas on completely overcast skies the amount of direct irradiance can be zero [14].

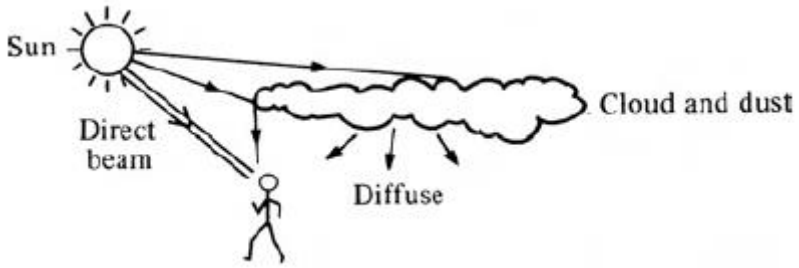

Figure 1 Origin of diffuse and direct beam radiation [14].

2.1.4 Standard spectrum

In rating the performance of photovoltaic modules a *Standard Spectrum* is used which assumes G of 1000 W/m^2, ambient temperature $T_{ambient}$ of 25°C and set input values for the transmittance functions mentioned above. It is shown in Figure 2 over the wavelength range of 350-2500 nm [15].

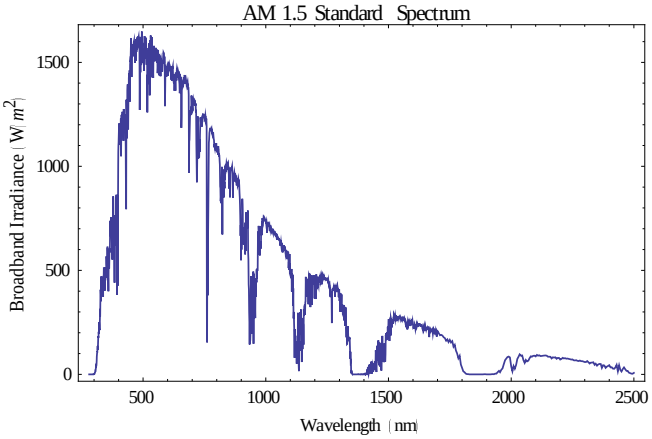

Figure 2 Standard spectrum used in rating photovoltaic modules [15].

2.1.5 Air mass effect on total irradiance

As solar radiation travels through the atmosphere it interacts with particles. Particles can cause the radiation to be scattered, reflected or absorbed. Subsequently, when the path of solar radiation in the atmosphere is increased, a net interaction with particles will also increase resulting in an alteration of G eventually reaching the earth's surface. Instead of working with the distance travelled through the atmosphere one can use the mass encountered by the solar radiation as a parameter to estimate to which degree G is altered as it passes through the atmosphere. The *air mass ratio* (*AM*) is a normalized unit used for this end. It has value 1 when the sun is overhead at an angle of 90° from the earth's surface and increases as the angle decreases.

A dominant scattering function is that of Rayleigh scattering. It is induced by particles which have a diameter that is the same as the wavelength of a photon interacting with it. Air particles have small diameters which correspond to that of photons with a short wavelength. Therefore as AM increases, so does the scattering of short wavelength radiation and as a result mostly longer wavelength photons will continue their direct (non-scattered) path towards the earth's surface. During sunrise and sunset, as opposed to mid-day, and more general during winter months, as opposed to summer months, *G* contains less short wavelength photons [14].

2.1.6 Cloud effect on total irradiance

Clouds mostly contain water particles which absorb solar radiation at varying wavelengths. In the visible spectrum the largest absorption takes place near the infrared, long wavelength region. During periods of overcast sky conditions, short wavelength photons are therefore overrepresented in the spectrum reaching the earth's surface as opposed to long wavelength photons [14].

2.1.7 Spectral responsivity

In semiconductors electrons are bound in the valence band. They can be excited to a free state in the conduction band only if they receive ample energy. This excitation can take place thermally or through the acquisition of energy from an incident photon. When an electron is excited to the conduction band the resulting absence of the negatively charged electron in the valence band results in a net positive charge being left behind. This positive charge can conceptually be considered as a *charge carrier* or "hole" which is free to move inside the valence band. Through the same reasoning electrons can also be considered charge carriers. The energy required to create this electron-hole pair is dependent on the semiconductor material and is represented by the so called band gap E_g. Subsequently only incident photons with energy $h\nu$ larger than or equal to the band gap of a semiconductor material will be able to contribute to the generation of an electron-hole pair. This photoinduced electron transfer is shown in Figure 3.

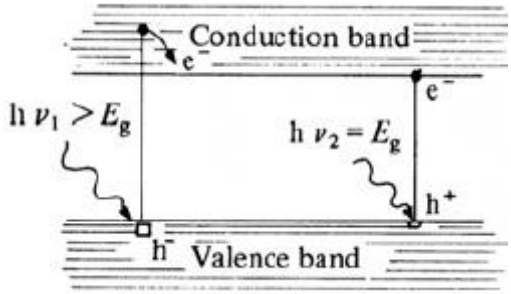

Figure 3 Incident photons of energy ≥ E_g will be able to generate an electron-hole pair [14].

The efficiency with which a material is capable of allowing photons of a certain wavelength to create an electron-hole pair is referred to as the *Internal Quantum Efficiency (IQE)* and is wavelength specific [12]:

$$IQE(\lambda) = \frac{\#\ of\ electron - hole\ pairs}{\#\ of\ incident\ photons(\lambda)}$$

Equation 5

With a plot of IQE set out against wavelength, the responsiveness of a solar module to certain ranges of spectral radiation can be made insightful. This is done in Figure 4 for typical PV

modules made of different semiconductor materials [16]. The figure shows that for some technologies the spectral response is narrow in the region of short wavelength/high energy photons (e.g. a-Si and CdTe). Other technologies have a broader response across a larger range of photon wavelengths/energies (e.g. CIS, CIGS and c-Si). Of course short/long and low/high here are relative to the chosen ranges.

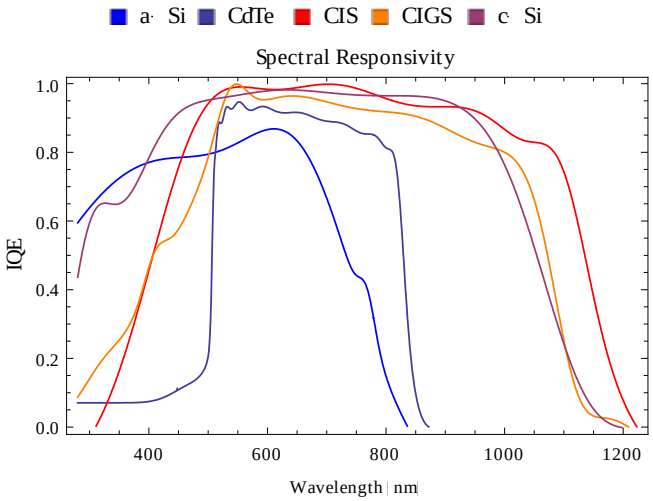

Figure 4 Spectral responsivity of different typical photovoltaic modules in terms of the internal quantum efficiency over a wavelength range [16].

2.1.8 Average photon energy

From the description of the IQE it is shown that not all photons can contribute to the generation of an electron-hole pair. The spectral irradiance at some wavelengths is more important than at others. Using the spectral irradiance at every individual wavelength to characterize the spectral distributions would however require laborious efforts to be taken. Instead, a single index of *Average Photon Energy (APE)* (in *eV*) can be used as a good indicator of spectral variation [17, 18]. The APE is defined as the average energy per photon which is included in the analysed spectrum and is calculated by division of the integrated irradiance over the integrated photon flux density:

$$APE = \frac{\int_a^b E(\lambda)d\lambda}{q\int_a^b \Phi(\lambda)d\lambda}$$

Equation 6

Here, q represents the electron charge (1.602*10-19 C) used for unit conversion from J to eV, and a and b are arbitrary wavelengths. The visible spectrum changing from blue to red as photon energy decreases leads to high values for APE corresponding to a "blue-rich" spectrum and low values for APE corresponding to a "red-rich" spectrum at equal broadband irradiance. The wavelength range used in this work is 350-1050 nm.

2.2 Photovoltaic power generation

2.2.1 Doping

In order to generate photovoltaic power with a semiconductor the material must be doped with impurity ions which change the valency of the intrinsic material and make it extrinsic. Ions with

a valency lower than that of the intrinsic material will result in a net majority of positive charge carriers. This is called p-doping and the ions are called acceptors (with concentration N_A) because they can "accept" an electron. Conversely doping the material with ions which have a higher valency will result in the material having a net negative charge. This is called n-doping and the ions are called donors (with concentration N_D) because they can "donate" an electron. Electrons on the n-side are referred to as majority charge carriers and holes are referred to as minority carriers. The opposite nomenclature holds for charge carriers on the p-side [19].

2.2.2 The *pn*-junction

In the region where p- and n-side semiconductors meet charge carriers start to flow. This region is referred to as the *pn*-junction. The difference in majority carrier concentrations, between the n-side and p-side, results in a diffusion of charge carriers towards the opposite side (electrons from n- to p- and vice versa for holes). This is called *electron/hole diffusion* and pertains to majority charge carriers. When charge carriers leave their initial location, they leave behind ionized dopant atoms (with concentrations of N_A^- on the p-side and N_D^+ on the n-side). The region where this occurs is called the *depletion region* because it is depleted of charge carriers. As a result of the absence of charge carriers an electric field is created which induces electrons to flow in the opposite direction of the diffusion flow. This flow is called *electron/hole drift* and pertains to minority charge carriers. Eventually an equilibrium situation is reached where the net flow of currents is zero. This occurs when the tendency of majority charge carriers to diffuse to a region of lower concentration density (diffusion) is exactly compensated by the counter-flow of minority charge carriers driven by the electric field (drift).
Diffusion current is often referred to as *recombination current* I_r. This nomenclature can be understood by realizing that recombination is driven by the concentration of minority charge carriers (majority charge carriers need minority charge carriers to recombine with). When a majority charge carrier diffuses across the pn-junction it becomes a minority charge carrier on the other side and will eventually recombine. Drift current is conversely often referred to as *generation current* I_g. In thermal equilibrium the net current is zero and recombination and generation therefore equate [14, 19];

$$I_r = I_g$$

Equation 7

2.2.3 Biasing

By connecting the ends of extrinsic materials with an external load the flow of charge carriers between the materials can be altered. Connection of the positive pole of the load to the p-side and the negative pole to the n-side creates an electric field, which opposes that in the depletion region. The applied bias is called a *forward bias*. The net electric field by such a bias is reduced and the diffusion current is increased. The drift current remains nearly the same because the number of minority charge carriers remains relatively unchanged. An opposite connection of the poles will create an electric field in the same direction as that near the depletion region and prevent majority charge carriers from diffusing to the other side. This applied bias is called a *reverse bias*. The diffusion current therefore decreases while the drift current again remains fairly unaltered [14, 19].

2.3 Performance

2.3.1 Circuit characteristics

Current, in the conventional form, flows away from the positive pole. A pn-junction under forward bias of V_b (>0), resulting in an increased recombination current, therefore becomes an increased forward current;

$$I_r = I_g * e^{qV_b/kT}$$

Equation 8

Where k is the Boltzmann constant ($1.38*10^{-23}$ m^2 kg s^{-2} K^{-1}) and the other quantities have been defined before. Without illumination the current I_D (or current in the dark) is the sum of the recombination and (negative) generation current;

$$I_D = I_r - I_g$$

$$I_D = I_g\left[e^{qV_b/kT} - 1\right]$$

Equation 9

This equation is known as the Schokley equation for the junction diode and is usually written in the form of Equation 10;

$$I_D = I_0\left[e^{qV_b/kT} - 1\right]$$

Equation 10

Here I_0 is the *saturation current* under full reverse bias and before avalanche breakdown.
Under illumination and forward bias charge carriers created through photoinduced electron-hole pair generation near the pn-junction are swept across by the electric field and result in a photon-generated current (I_L or I_{ph}). The solar cell current (I) is therefore the sum of the dark current and the (negative) photon-generated current;

$$I = I_D - I_L$$

$$I = I_0\left[e^{qV_b/kT} - 1\right] - I_L$$

Equation 11

Figure 5 shows the characteristics of a pn-junction in the dark and under illumination with an increase of I_D as forward bias is increased. Illumination causes a solar cell to behave as a power source. In a discharging battery, electrons flow from the negative pole to the positive pole. The bottom sketch of Figure 5 shows that illumination of the solar cell results in a photon-generated current in which electrons flow towards the negative pole, charging the battery (and thus generating power) [14, 19].

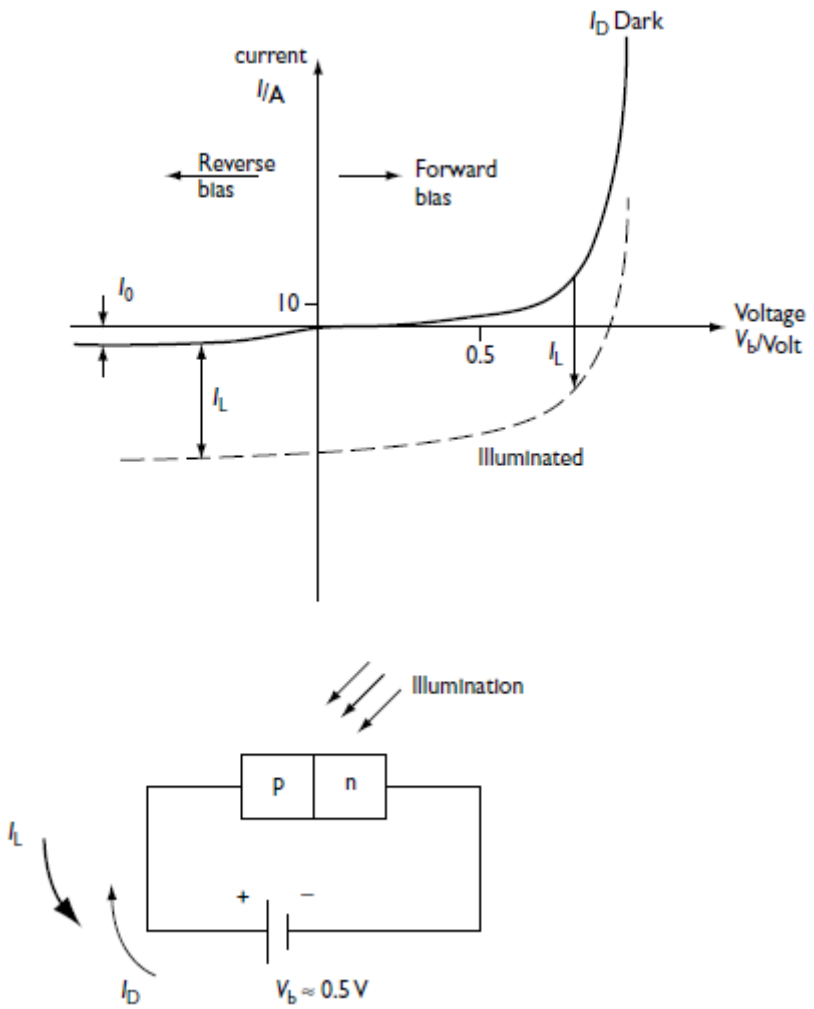

Figure 5 The negative discharging character (i.e. charging) of a pn-junction under illumination, illustrated by the top plot where illumination results in the line moving in the fourth quadrant with negative current, proves that a solar cell under forward power produces power. The bottom sketch shows the pn-junction in a circuit diagram with the dominant currents flowing as a result of the applied forward bias V_b and illumination [14].

Because a PV module generates power the IV-characteristics of a pn-junction are generally flipped along the x-axis, placing quadrant 4 in quadrant 1. Power being a product of current and voltage and the characteristics of a pn-junction being non-linear imply that a trade-off must be made between the applied bias and its resulting current output in order to achieve a maximum amount of power output. This is shown in Figure 6. The current and voltage at which maximum power is reached (P_{MP}) are referred to as I_{MP} and V_{MP} respectively. Maximum current is achieved at zero bias voltage (I_{SC}) and maximum voltage is reached at open circuit conditions (V_{OC}). I_{SC} and V_{OC} are generally used as parameters for quantifying module performance as opposed to I_{MP} and V_{MP}, in part because the latter can't be determined analytically.

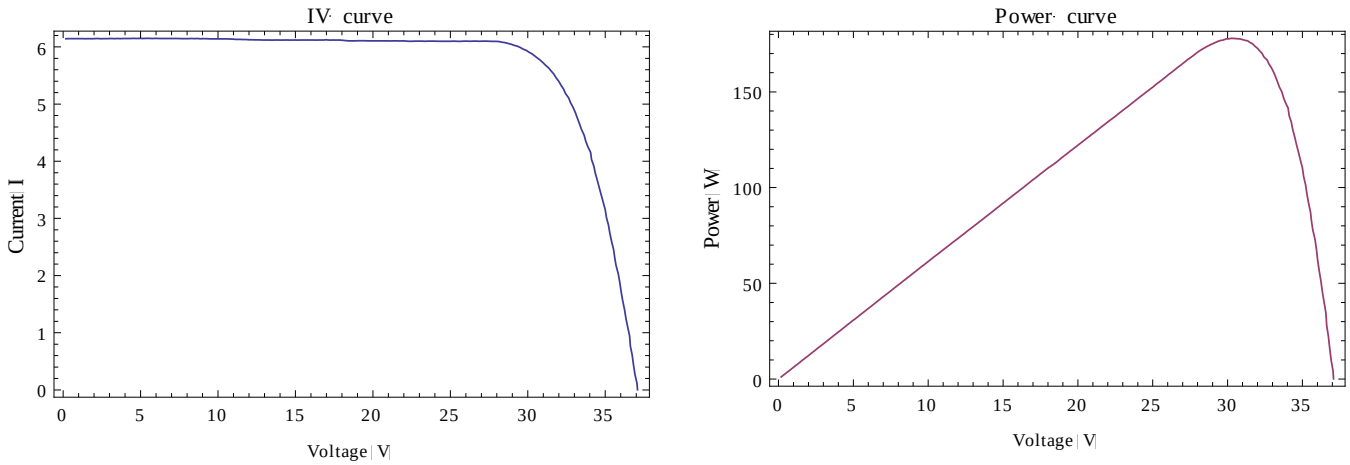

Figure 6 IV-characteristic of a PV module and the resulting power curve which gives the amount of power when the bias voltage is altered.

An increase in module temperature has a positive effect on I_{SC} and a negative effect on V_{OC}. The effect on V_{OC} however is larger than that on I_{SC} resulting in a net negative effect of temperature on the power output. The temperature dependency of V_{OC} is elaborated on in more detail in the appendix.

2.3.2 Performance Ratio

In order to compare different PV modules which operate under varying climatic conditions an indicator is necessary which corrects for performance under non-STC conditions. One such indicator is the *Performance Ratio* (*PR*) [20]. It gives the ratio between the final system (or module) yield ($E_{feed-in}$);

$$E_{specific} = E_{feed-in}/P_{STC}$$

Equation 12

and a reference yield under STC ($H_{specific}$);

$$H_{specific} = H_{POA}/G_{STC}$$

Equation 13

Here, P_{STC} and G_{STC} refer to power output and total irradiance under STC. $E_{feed-in}$ and H_{POA} stand for the measured power output and total irradiance measured on the plane of array respectively. The resulting PR is a dimensionless measure of module performance;

$$PR = E_{specific}/H_{specific} * 100\%$$

Equation 14

As mentioned earlier, current and voltage (and thus power) are affected by changes in temperature. Manufacturers generally quantify this effect in terms of temperature coefficients which give the losses (or gains) in current, voltage and power when modules operate under temperatures which deviate from STC ($\frac{dx}{dT}$). Accounting for losses in power yields the following equation;

$$E_{feed-in} = P_{mp} * \left(1 + \gamma_{mp} * (T_{module} - T_{STC})\right)$$

Equation 15

Here, γ_{mp} is the negative temperature coefficient for power, T_{module} is the measured module temperature and T_{STC} refers to the module temperature at 25°C. Temperature corrections for I_{SC} and V_{OC} are performed in a similar fashion with the temperature coefficient for V_{OC} being

negative also and that for I_{SC} being positive. Coefficient values for I_{SC}, V_{OC} and P_{mp} of one of the mono-Si modules used in this work for instance are 0.0004, -0.0036 and -0.0043 respectively. Values for an a-Si module are 0.0004, -0.0024 and -0.0025 respectively. Differences between technologies can therefore be significant.

3 Methods

3.1 Experimental setup

The test facility is located on the rooftop of the eight storey Hans Freudenthal building of the Utrecht University (52.09°N, 5.17°E). It was designed for the purpose of assessing the performance of 24 commercially available PV modules under outdoor weather conditions [11]. The setup is positioned according to the solar azimuth and plane of array angles of 180° and 37° respectively. There are two inverters present, each being connected to 12 PV modules.

3.2 Measuring equipment

With the exemption of the weather station, which is fabricated by Lufft GmbH, all measuring equipment is designed by EKO Instruments [21, 22]. Both in-plane and horizontal irradiance measurements as well as weather measurements are being performed on a one minute interval basis. Module performance measurements have a three minute interval resolution and are only performed at irradiance levels exceeding 50 Wm^{-2}. The measurements of the in-plane irradiance are synchronized with those of the module performance. The setup is shown in Figure 7.

3.2.1 Pyranometers

Two MS-802 pyranometers are located at the UPOT. One measures the in-plane global irradiance (H_{POA}) in the range of 305-2800 nm and the other measures the horizontal global irradiance in the same range.

3.2.2 Spectroradiometer

To measure the spectral irradiance a MS-700 spectroradiometer is used. Its operating spectral range is 350-1050 nm with a spectral resolution of 3.3 nm. It is mounted in-plane and its detector exposure time is automatically adapted between 10 msec to 5 sec to optimize the signal to noise ratio.

3.2.3 Sun tracker

A STR-22G sun tracker is mounted with both a MS-56 pyrheliometer and a MS-402 pyranometer and has an angular resolution of 0.009°. The path of the sun can be determined by two independent modes. The first mode tracks the exact solar position through a sun sensor. The second mode calculates the solar position through a solar algorithm. When the sun is absent the calculation mode will only be activated.

3.2.4 Pyrheliometer

A MS-56 pyrheliometer is mounted on the sun tracker to measure the direct normal irradiance (I_{direct} or DNI). It measures irradiance in the range of 200-4000 nm and therefore covers the entire spectral range of all installed PV modules.

3.2.5 Pyranometer

A MS-402 pyranometer is mounted together with a shading ball on the sun tracker to measure the diffuse irradiance ($I_{diffuse}$). Its range of measured irradiance being 305-2800 nm differs from that of the pyrheliometer but also covers the entire spectral range of all the installed PV modules

3.2.6 Weather station

A WS600-UMB weather sensor is installed to measure climatic conditions which include air temperature, relative humidity, precipitation intensity, precipitation type (rain or snow), precipitation quantity, air pressure, wind direction and wind speed.

Figure 7 Pictures of the UPOT on a clear sky day.

3.3 Modules

The modules located at the test facility pertain to different technologies and brands. Two types of each module were installed and connected to the two separate inverters (channel 1 and channel 2). The modules investigated (10 in total) are made from different materials; mono-Si (three types referred to as A, B and C), poly-Si (two types referred to as A and B), a-Si, CdTe, CIGS, HIT and CIS.
For most modules measurement data collected from the modules connected channel 1 only have been chosen for analyses. The reason for this is that the performance, in terms of I_{SC} and V_{OC}, between each individual module in these sets did not differ significantly. For the mono-Si A data from channel 2 was chosen because the module connected to channel 1 gave bad measurements for some days.

3.4 Data

3.4.1 Availability

For the selection of time periods to be analysed measurement values of I_{direct} have been used. Seeing as the sun tracker and pyrheliometer were installed on 2013-03-20 any measurements from before this date have not been incorporated in the analysed dataset. Construction work on the terrain of the University Utrecht furthermore resulted in a large construction crane being position south of the test facility in front of the Hans Freudenthal building. The end of the crane being able to move straight over the test facility and the base being positioned right in front of it resulted in frequent shadows being casted over the modules and measuring equipment (Figure

8). For this reason measurements dating from 2013-11-05 onward, when the crane was put in place, have also not been incorporate in the analysed dataset.

Figure 8 Pictures of an obstructed view at UPOT with the crane casting a shadow over the modules and measuring equipment and hanging directly over the test setup.

A preliminary analysis of the weather data showed unexpected precipitation measurements having been recorded in the month August. This is shown in Figure 9. Values were higher than expected and differed from measurements taken from a nearby meteorological weather station. Values from the other months showed good resemblance. For this reason precipitation measurements taken in the month August have been excluded from the dataset.

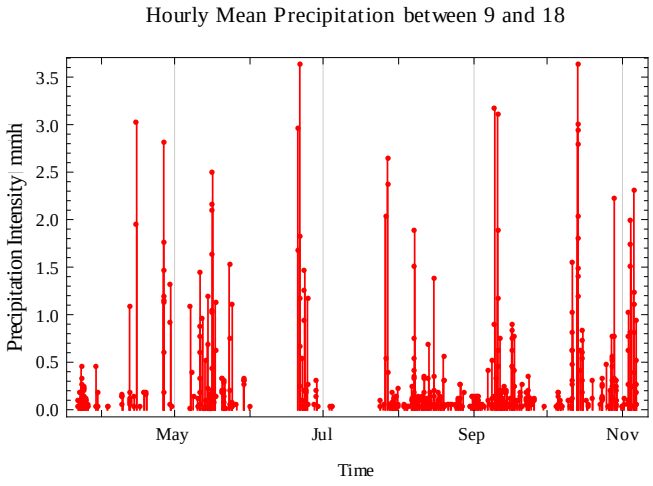

Figure 9 Irradiance profile measured at UPOT with the month August showing unexpected high values.

3.4.2 Acquisition

A MySQL database is used to store the data collected at UPOT which is acquired with the help of Labview software [23]. Wolfram Mathematica 9.0 has furthermore been used in this work to analyse and interpret the data [24].

3.5 Weather classification

Cloud cover is often measured in oktas which depend on a visual interpretation of the sky. Given the laborious effort it would require to interpret cloud cover on this scale for every timestamp (performance and irradiance measurements have a granularity of a few seconds) a cloud cover

classification system has been implemented which uses physical properties as inputs. The system uses a so called "Arrow Head" scatter plot, as first proposed by Stein et al., to give a representation of the cloud cover [25]. This scatter plot is built up by two parameters; the clearness index and the variability index. Both these parameters are calculated based on irradiance values during a clear sky day. For this purpose the SPCTRAL2 clear sky model has been used which estimates both direct and diffuse irradiance. Given the lack of accurate inputs which are needed for the calculation of the diffuse component, the modelled irradiances presented in this work refer to the direct component only.

3.5.1 SPCTRAL2 clear sky model

The SPCTRAL2 model was developed with the goal of providing researchers with the capabilities to calculate spectral irradiance at different geographic locations and under different atmospheric conditions [13]. The model uses atmospheric, geographic and geometric input parameters to calculate irradiance levels for 122 wavelengths at varying intervals in the range of 300 to 4000 nm. These inputs are relative humidity, air pressure, ambient temperature, zenith angle, air mass and datetime. SPCTRAL2 being a spectral model requires model outputs to be integrated in order to obtain direct irradiance values. Furthermore a first order linear interpolation was applied to estimate irradiance values in between the calculated 122 wavelengths.

3.5.2 Clearness Index

The clearness index is a parameter which indicates the irradiance intensity. It gives the ratio between the measured direct irradiance $I_{D,meas,t}$ during a certain time interval T and the modelled direct irradiance $I_{D,mod,t}$ during the same interval and is given by:

$$CI = \frac{\sum_{t=1}^{T} I_{D,meas,t}}{\sum_{t=1}^{T} I_{D,mod,t}}$$

Equation 16

A value of 1 implies that the $I_{D,meas}$ is the same as that on a clear sky day ($I_{D,mod}$). Lower values refer to time intervals in which more cloud cover is present. Values exceeding 1 refer to time intervals in which $I_{D,meas}$ is higher than $I_{D,mod}$ but both are low. These intervals can occur around sunrise and sunset when the model outputs are less accurate. Figure 10 shows a day (2013-06-07) in which CI for most time intervals would have a value of 1 because $I_{D,meas}$ and $I_{D,mod}$ are near equal throughout the day.

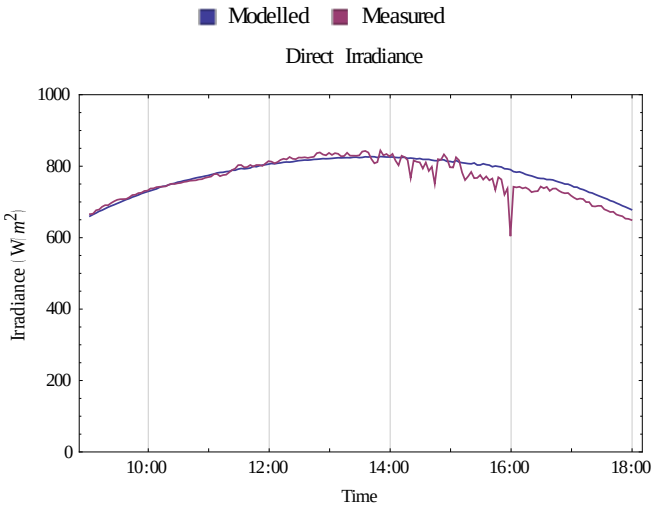

Figure 10 Example of a day on which the value for CI is near unity for the entire day.

3.5.3 Variability Index

The variability index is a parameter which indicates the irradiance variability. It was first proposed by Stein et al. and can be conceived conceptually as the ratio between two lines; the "length" of $I_{D,meas}$ plotted against time and the "length" of $I_{D,mod}$ plotted against time. It is given by:

$$VI_{Stein\ et\ al.} = \frac{\sum_{k=1}^{n}\sqrt{\left(I_{D,meas,k} - I_{D,meas,k-1}\right)^2 + \Delta t^2}}{\sum_{k=1}^{n}\sqrt{\left(I_{D,mod,k} - I_{D,mod,k-1}\right)^2 + \Delta t^2}}$$

Equation 17

where the iterator *k and k-1* represent consecutive measurements taken in the time interval *Δt*. This variability index has been adjusted in two manners. First, seeing as the representation of cloud variability by means of the "length" of two lines has no physical meaning (i.e. $\sqrt{\left(\frac{W}{m^2}\right)^2 + s^2}$ is not a physical unit) the variability index used in this work is adjusted to exclude the time component. Second, dividing the absolute differences in irradiance would yield very high values for days with partial cloud cover making comparisons between different days difficult. The square root of the ratio is therefore taken in order to group the extreme values and maintain a distinction between days in which the variability in irradiance is relatively low. The variability index used therefore becomes:

$$VI = \sqrt{\frac{\sum_{k=1}^{n}\left(I_{D,meas,k} - I_{D,meas,k-1}\right)}{\sum_{k=1}^{n}\left(I_{D,mod,k} - I_{D,mod,k-1}\right)}}$$

Equation 18

Low values for VI imply that the development of irradiance levels is gradual or very low. This occurs during clear or highly overcast time intervals. High values for VI imply that the variability in irradiance is high and clouds are therefore relatively small and move across the sky with a high velocity. Figure 11 shows a day (2013-05-24) in which VI for most time intervals would have a relatively high value because $\sum_{k=1}^{n}\left(I_{D,meas,k} - I_{D,meas,k-1}\right)$ >> $\sum_{k=1}^{n}\left(I_{D,mod,k} - I_{D,mod,k-1}\right)$ throughout the day.

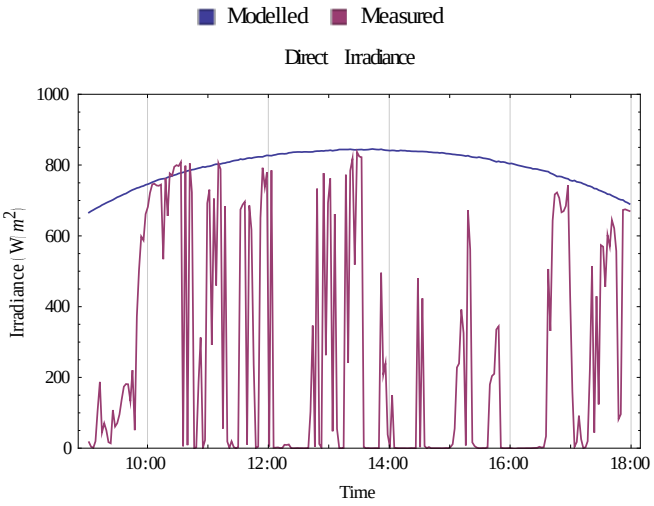

Figure 11 Example of a day on which the VI is high throughout the entire day.

3.5.4 Scatter plot interpretation and validation

The time horizon chosen to calculate the CI and VI for is one hour. Measurements for $I_{D,meas}$ are performed on a one to three minute interval basis and therefore result in 20-60 data inputs per calculation. Calculations done for a shorter time horizon presumably would not yield enough data points for the results to be reliable. Three cloud cover types can be distinguished through an interpretation of the scatter plot;

- A clear sky, where CI has a value around 1 and VI is low
- A (uniformly) overcast sky, where CI has a value around 0 and VI is low
- A non-uniform sky, where CI has a value between 0 and 1 and VI is relatively high

Figure 12 shows a typical days which correspond with each of the described cloud cover types; 2013-06-07 (clear sky or type 1), 2013-11-02 (overcast sky or type 2) and 2013-05-24 (non-uniform sky or type 3). The top three plots give the development of the Global Irradiance throughout the day. The bottom plots show the associated scatter plots and confirm the categorization method described above.

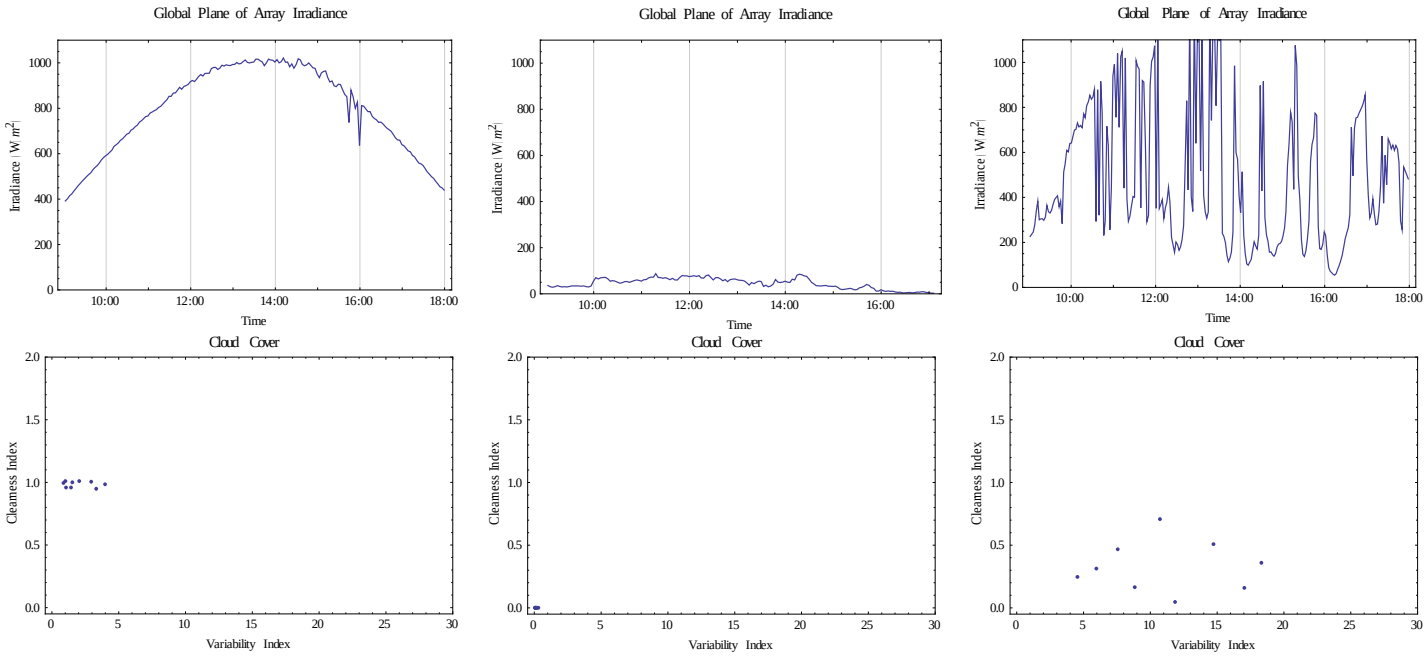

Figure 12 Examples of three of the described days and their corresponding cloud cover types presented in an arrow head scatter plot.

For the period 2013-03-21 till 2013-11-05, which includes a large part of spring, summer and autumn, it is shown in Figure 13 that clear and overcast sky hours are predominant. This does however not necessarily say that the same holds for entire days but it does confirm that the performance analysis of PV modules during overcast hours is relevant for the Netherlands. Hours chosen are those where between 09:00h and 18:00h (daytime hours).

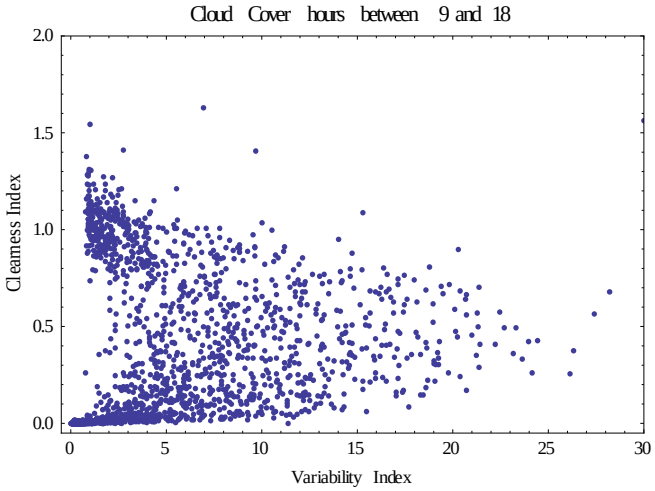

Figure 13 Arrow head scatter giving the cloud cover for the period 2013-03-21 till 2013-11-05 with the exemption of the month August.

Figure 14 shows the cloud cover for hours in which rainfall was measured. The colour of the data points in the scatter plot correspond to the precipitation intensity ranging from low (yellow) to high (red). Hours chosen here are also only daytime hours. The cluster of data points near the origin of the left scatter plot indicate that precipitation predominantly occurs in hours in which skies are overcast. The right plot, which focusses on the origin of the left plot, shows that high precipitation levels occur during hours of highly overcast skies. This means that if the effect of precipitation on PV module performance is to be investigated, a comparison of highly overcast hours with and highly overcast hours without precipitation would seem logical. Doing

so would ensure that cloud cover, and thus irradiation levels, for those hours are similar and the effect of irradiance on PV module performance is eliminated.

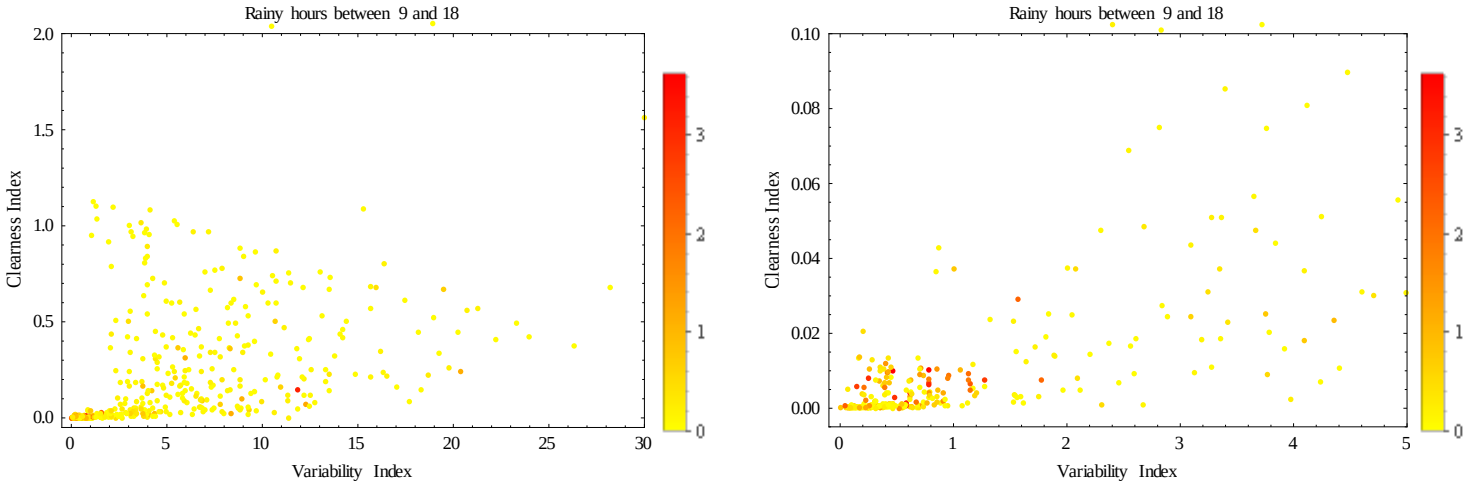

Figure 14 Cloud cover plots combined with hourly mean precipitation intensities. The plot on the left shows that hours in which precipitation is measured can often be described as overcast (the cluster near the origin of the plot). The plot on the left is zoomed in on said region and the red colour of the data points indicate that hours in with a high mean value for precipitation intensity are often overcast hours.

3.6 Day selection

The selection of time periods to be added to the dataset has eventually been done using three parameters: $\mathbf{H_{POA}}$ (<250 Wm^{-2} for at least two consecutive hours), **cloud cover type** (overcast or type 2) and **precipitation** (measured or not measured). Figure 15 gives an example of both a rainy and non-rainy time period which has been incorporated in the analysed dataset and shows the values for the three aforementioned parameters. A list of all the time periods added to the dataset can be found in section 8.2

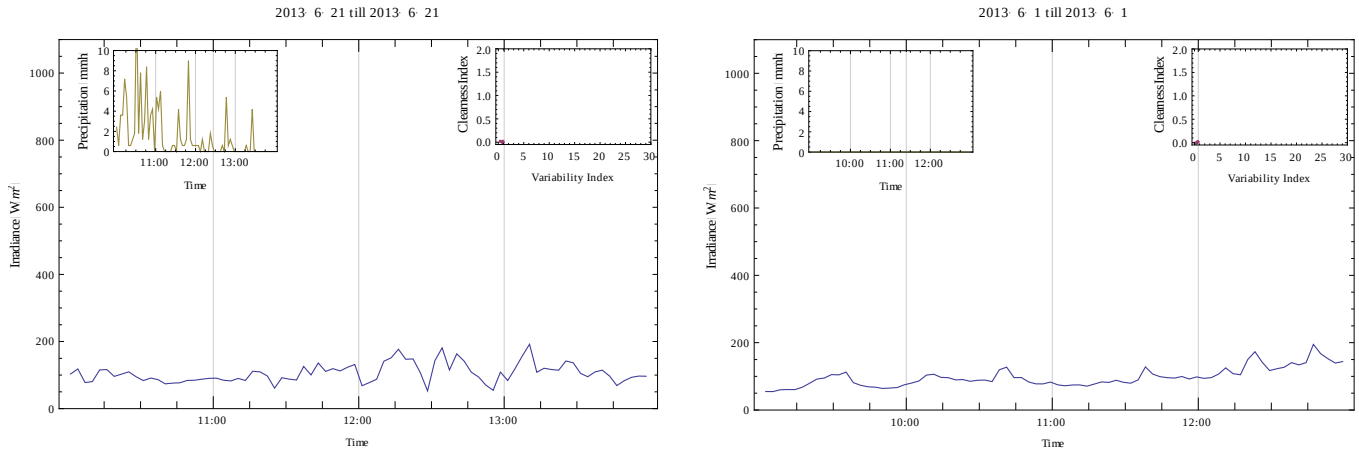

Figure 15 Examples of two time periods which are incorporated into the dataset (left for the rainy and right for the non-rainy time period). The small graphs in the upper left corner of the plots show the precipitation intensity and the upper right graphs show the values for CI and VI.

4 Results

The results are structured in line with the research questions set out section 1.2

4.1 Effect on physical module properties and climatic conditions

4.1.1 Effect on T_{module}

The plots on the left of Figure 16 account for $T_{ambient}$, by selection of hours in which $T_{ambient}$ remains constant, and illustrate that as the precipitation intensity increases, T_{module} decreases and that this is not caused by a decrease in $T_{ambient}$. The middle plots account for irradiance and illustrate that in periods of relatively low to no precipitation T_{module} is driven by H_{POA} and that this mechanism is reduced in periods of increased precipitation intensity. The plots on the right finally account for wind speed. Analysing the top right plot one could argue that the decrease in T_{module} is attributable to an increase in wind speed. The bottom right plot however shows that on a day in which the wind speed remains fairly constant T_{module} increased in the hours in which no precipitation was measured. These observations indicate that rainfall lowers $T_{module.}$ The measurements presented in Figure 16 pertain to those recorded for the CdTe module. The cooling effect of precipitation was however noticed for all modules.

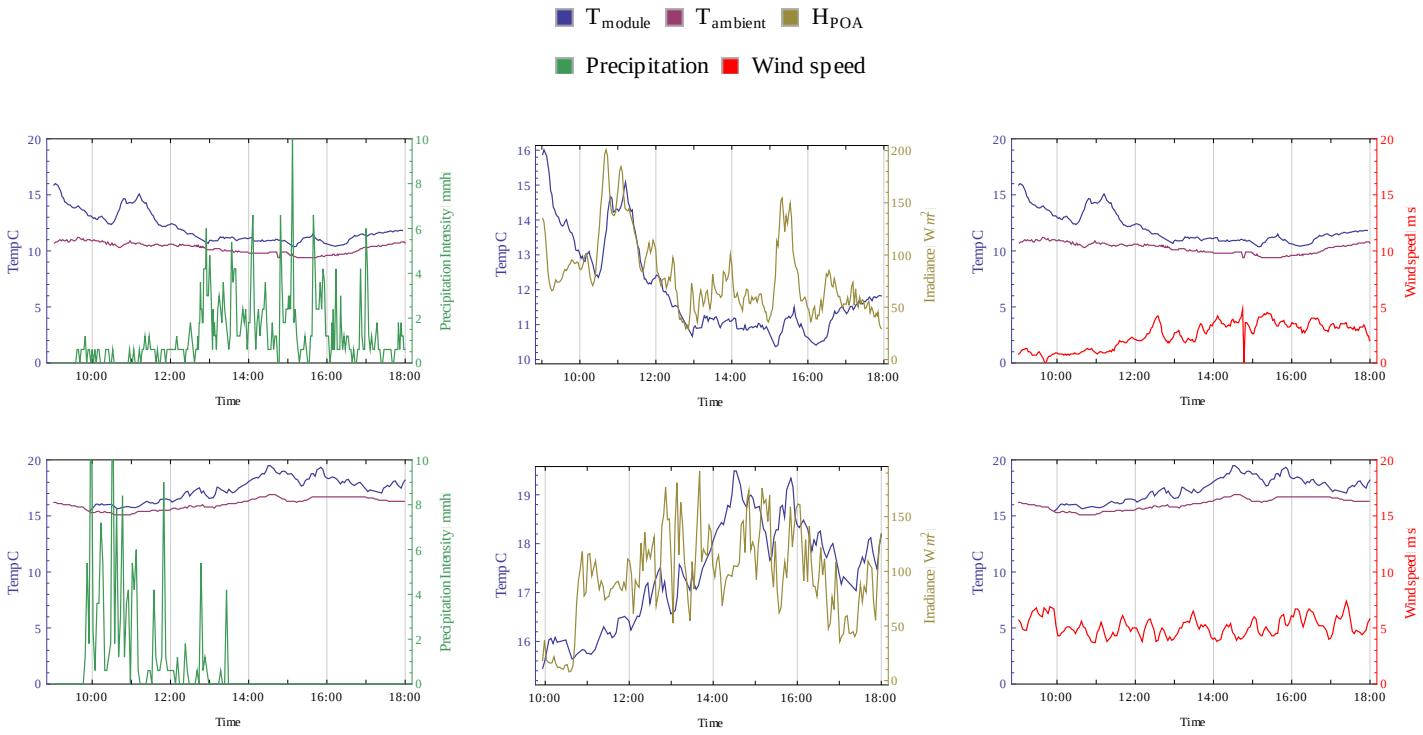

Figure 16 The effect of precipitation on T_{module} during two separate time periods. In the left plots, during high levels of precipitation (green lines), the difference between $T_{ambient}$ (blue lines) and T_{module} (red lines) becomes smaller indicating a cooling effect induced by precipitation. In the middle plots, changes in irradiance (gold lines) are accounted for and it is shown that precipitation limits the H_{POA} to warm the module. The plots on the right show that the decrease in T_{module} is not necessarily caused by an increase in wind speed (green lines).

As mentioned in 2.3.1 a decrease in T_{module} will lower I_{SC} and increase V_{oc}. Precipitation induced changes in T_{module} therefore affect the IV-characteristics of a PV module.

4.1.2 Effect on spectrum

From approximately 2000 measurements of the APE it is noticed that precipitation changes the composition of spectral irradiance. Figure 17 shows this observation and relates it to the spectral responsivity of some typical solar modules. The left plot shows that the mean APE is higher during rainy (green line) than during non-rainy (orange line) time periods. The right plot shows the distribution in recorded APE values for all the time periods investigated. This indicates that precipitation causes the spectrum to shift towards the blue. The non-vertical lines in Figure 17 show that, in the investigated region, the IQE increases for the a-Si and CdTe modules and that for the other modules the IQE remains fairly constant. A higher IQE indicates that more electron-hole pairs will be generated resulting in an increased electron current and a subsequent increase in I_{SC}. Precipitation will therefore presumably have a positive effect on the I_{SC} of a-Si and CdTe modules.

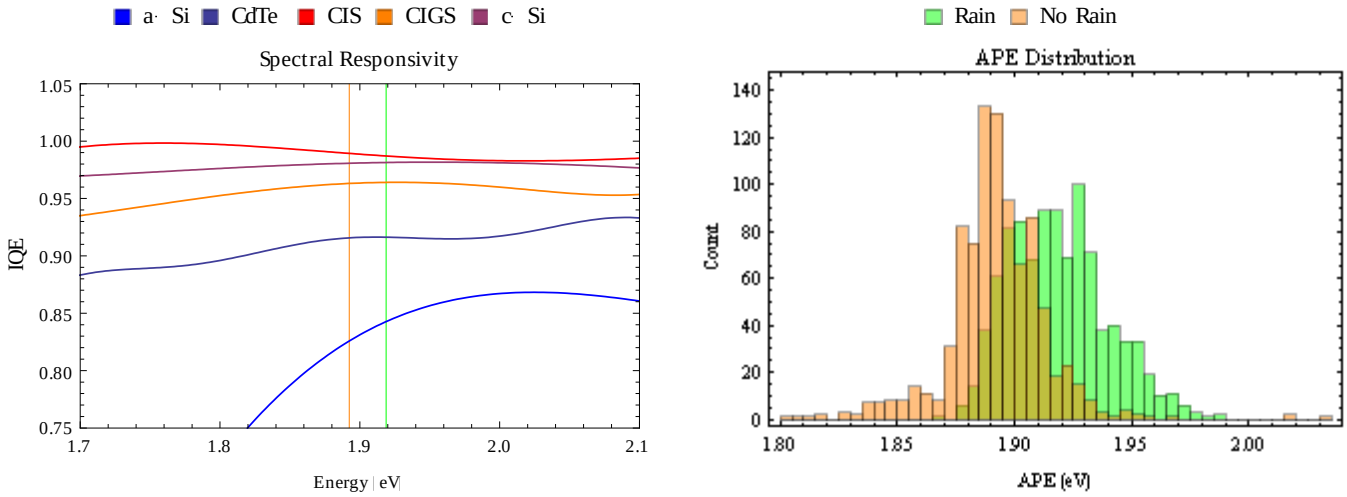

Figure 17 The left plot shows mean APE values for rainy (green) and non-rainy (orange) time periods compared to spectral responsivity of typical PV modules. The right plot shows the distribution in APE values. The figure shows that a) mean APE values are higher during rainy time periods and that b) IQE (and thus I_{SC}) increases for a-Si and CdTe modules as APE increases in the measured regions and that for the other modules the difference in IQE is less noticeable or even negative.

4.1.3 Effect of precipitation intensity

As can be found in many thermodynamic textbooks elongated contact of a heat source (i.e. warm PV module) with a heat sink (i.e. cold rainwater) will result in an increased cooling effect as the thermal conductivity of water is much higher than that of air. From 0it therefore follows that an increased intensity in precipitation will result in an increased V_{OC}.

The intensity effect on I_{SC} however is not that straightforward on forehand. It may be possible that water droplets (during low levels of precipitation) or a water film (during high levels of precipitation) present on a PV module's front glass cover alter the ratio between the amount of absorbed and reflected photons and thereby affect the I_{SC}. The *external quantum efficiency* (EQE) is a measure often used to describe such losses or gains. It gives the ratio between the amount of charge carriers created and the incident amount of photons, just like the IQE, but also accounts for reflection losses. Because measurements of both the IQE and EQE require complicated setups the intensity effect on I_{SC}, possibly caused by an increased reflection of incident solar radiation, is investigated through a direct analysis of I_{SC}. A comparison of three time periods, in which

precipitation intensity differed and all other known affecting parameters remained constant (APE and H_{POA}), was made to this end. The values for precipitation intensity, APE and H_{POA} can be found in Figure 23 section 8.2

In Figure 18 H_{POA} is set out against I_{SC} for the three time periods with different precipitation levels. The a-Si and CdTe modules are presented here because of their presumed higher sensitivity to changes in the spectral composition. The mono-Si B and CIGS modules are shown because their performance, in terms of I_{SC} and V_{OC}, correspond to that of most of the other investigated modules. Plots for the other modules can be found in Figure 24 section 8.3 It can be seen that the intensity differences do not result in significant changes in I_{SC} (the regression lines overlap). This shows that, other than through a change in the spectral irradiance and the total irradiance, precipitation intensity has no clear effect on I_{SC}.

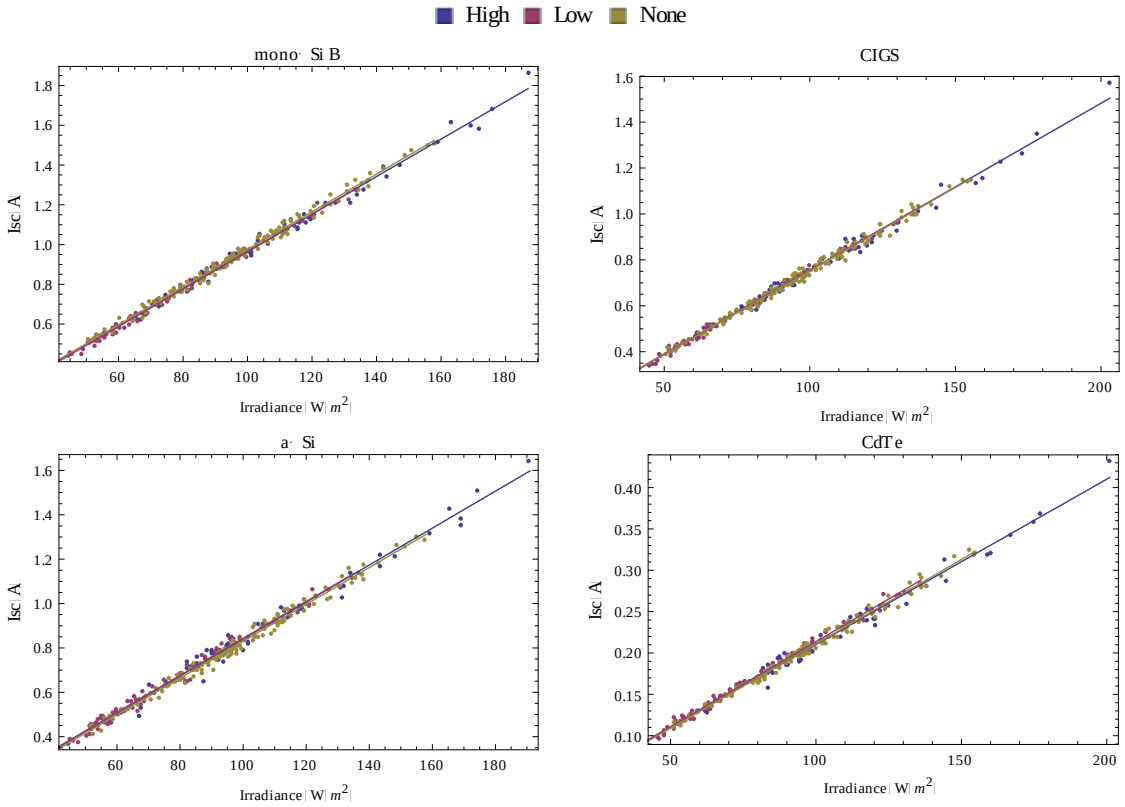

Figure 18 Temperature corrected values for I_{SC} set out against H_{POA} under equal levels of mean APE and three different levels of precipitation. The overlap in regression lines shows that the intensity of precipitation has no clear effect on I_{SC}.

4.2 Effect on performance

4.2.1 Effect on I_{SC}

As mentioned before, two opposing mechanisms will have an effect on the I_{SC} of a module under precipitation; a temperature induced decrease due to the cooling effect (small for all modules) and a spectral shift induced increase (significant for some modules). Figure 19 shows the temperature corrected values of I_{SC} set out against H_{POA} for the same four modules as presented in the previous section. Plots for the other modules can be found in section 8.4 Using these values instead of the non-corrected ones ensures that, if it is assumed that the temperature coefficients are accurate and no other mechanisms are at play, the effects of the second mechanism (spectral shift) will become apparent. This mechanism is shown in Figure 19; both the a-Si and CdTe modules under rainy weather conditions outperform those under non-rainy weather conditions.

What furthermore becomes clear is that the other modules, which according to Figure 17 should not be as sensitive to changes in the spectrum, also perform slightly better under rainy weather conditions. It should be noted that the spectral responsivity curves shown earlier pertain to typical modules for each technology. The specific responsivity of the investigated modules could therefore be such that they, just like the a-Si and CdTe modules, perform better under rainy weather conditions in which the APE is generally higher. This could then explain the difference in I_{SC} performance between the two weather conditions. If not then there is some other undefined mechanism which results in this difference.

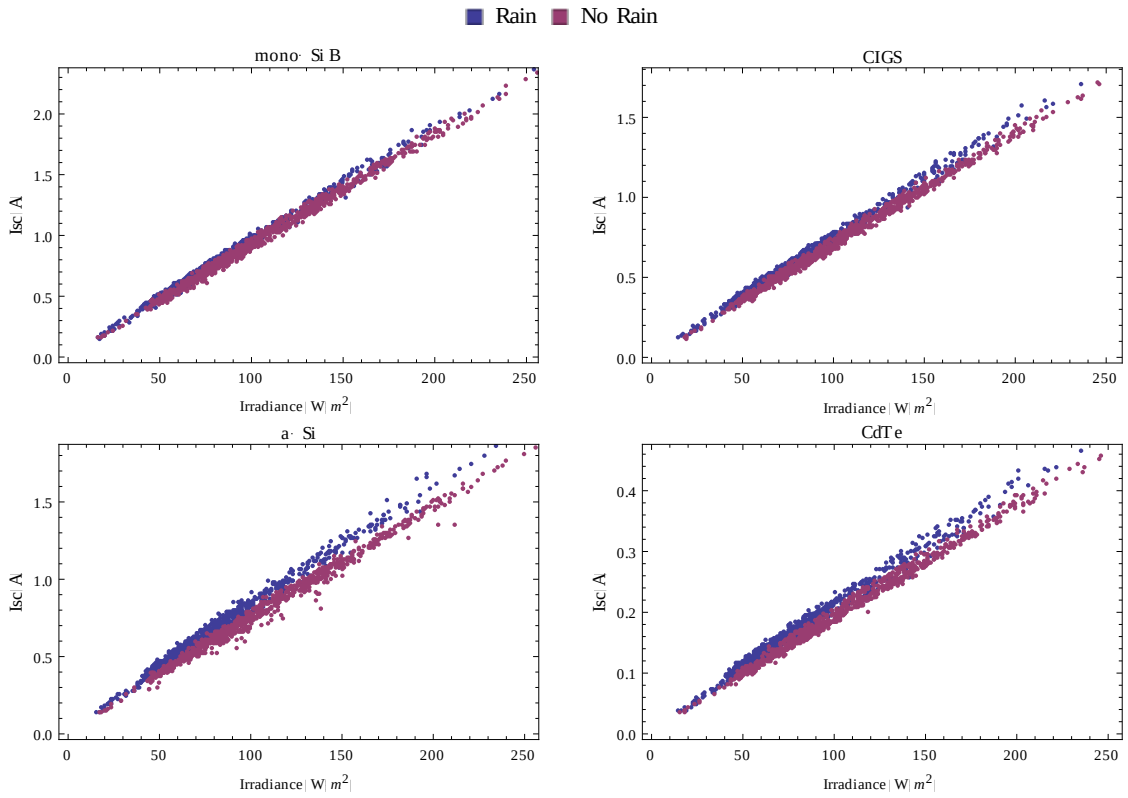

Figure 19 Temperature corrected values for I_{SC} set out against H_{POA} under rainy and non-rainy time periods. The blue data points having a higher value for I_{SC} at same levels of H_{POA} indicate that, as expected, the a-Si and CdTe modules perform better under rainy than under non-rainy weather conditions.

4.2.2 Effect on V_{OC}

Figure 20 shows measurements of V_{OC} set out against H_{POA} for the same four modules as presented in the previous sections. In sections 8.5 and 8.6 the plots for all the other modules can be found. The left plots correspond to the non-temperature corrected values and show that during rainy time periods V_{OC} is generally higher than during non-rainy time periods. Given the temperature dependence of V_{OC} this result is to be expected. For this reason the plots on the right present temperature corrected values for the same time periods. If the applied temperature coefficients are accurate and no other major mechanisms are at play then the data points in these plots should lay on the same regression line. Figure 20 however clearly shows that the rainy data points lay above the non-rainy data points. A plausible explanation for this observation is that the temperature measurements are inaccurate because of a delay in temperature change. The temperature sensor is located on the back side of each solar module. The thermal conductivities of the different materials comprising the module are such that changes in temperature occurring at the front end, due to precipitation, will not immediately result in a drop in temperature at the back where the sensor is positioned. This delay in temperature drop will mean that recorded temperatures are too high and subsequently result in temperature corrections being too severe (i.e. the rainy data points are too high).
What can furthermore be seen in Figure 20 is that the difference in rainy and non-rainy V_{OC} for the a-Si and CdTe modules is significantly higher than the difference for the other modules. Recalling both Equation 19 (which shows that an increase in I_{SC} will result in an increase in V_{OC}) and the observed increase in I_{SC} during rainy time periods from the previous section explains this residuary non-congruent pattern in V_{OC}.

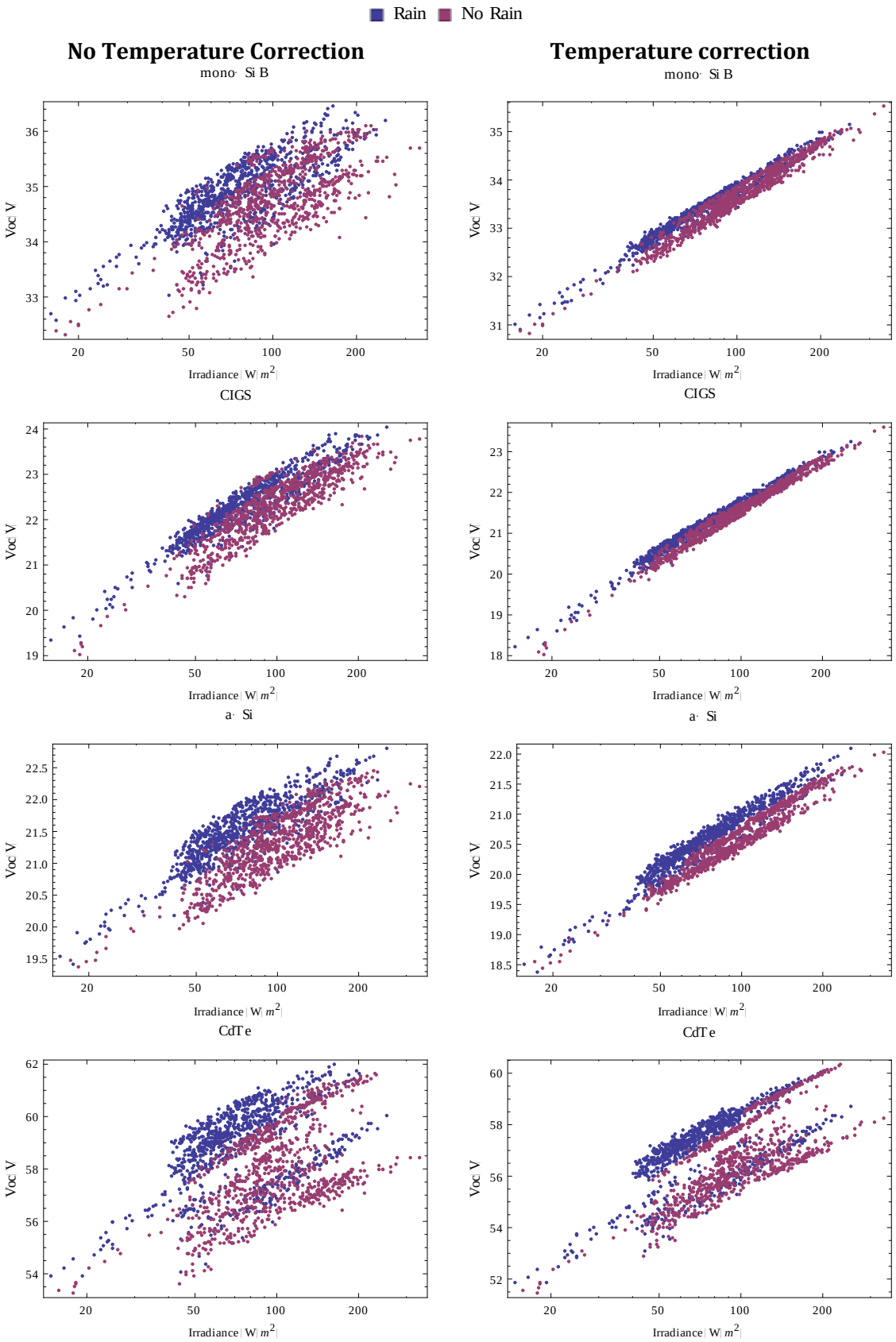

Figure 20 Temperature corrected values for V_{OC} (logarithmic scale) set out against H_{POA} under rainy and non-rainy time periods. Temperature having a dominant effect on V_{OC} should result in temperature corrected values for rainy time periods being similar to those of non-rainy time periods. The blue rainy data points having a higher value at than the non-rainy data points suggest that temperature measurements are inaccurate (too high resulting a correction which is too small). The values for the a-Si and CdTe modules are expected to be slightly higher due to increased I_{SC}.

4.2.3 Effect on PR

Figure 21 shows the difference in PR under rainy and non-rainy weather conditions for each of the investigated modules ($\Delta PR = PR_{rain} - PR_{no\,rain}$) where PR calculation have been performed according to Equation 14 and pertain to mean values of both datasets.
If the results for the poly-Si A and CIS modules are neglected the ΔPR values for all other modules can be understood from a consideration of the previous results; a) all modules have a slightly higher V_{OC} during rainy weather periods, due to a delay in recorded temperature drop, resulting in ΔPR of a few percent for all modules and b) the a-Si and CdTe modules have a higher I_{SC} and V_{OC} during rainy weather conditions due to changes in the spectral irradiance resulting in even higher values for their ΔPR.

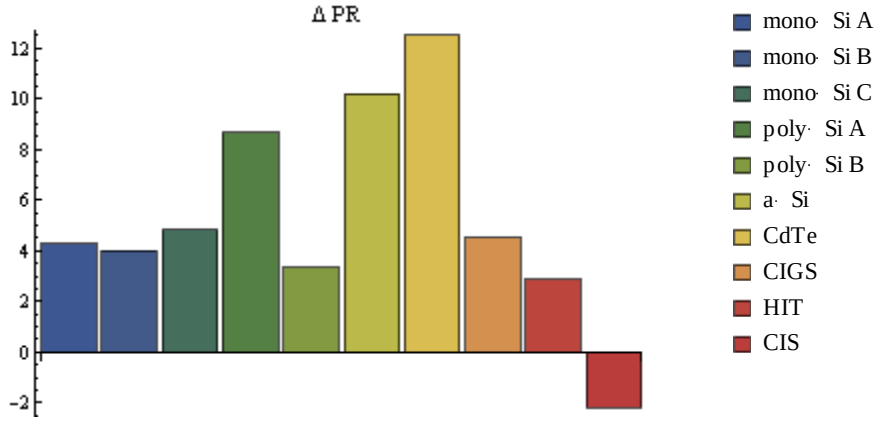

Figure 21 Difference between rainy and non-rainy PR for all investigated modules. Part of the higher PR during time periods of precipitation can be explained by a delayed drop in temperature measured at the back of the module; temperature corrections are too high resulting in the calculated PR being too high also. The higher PR for the a-Si and CdTe modules can be attributed to the increased measured I_{SC} during rainy time periods.

The poly-Si A and CIS modules performing different than expected is also made apparent when looking at the distribution in ΔPR. Figure 22 shows the distribution of the poly-Si A, CIS, a-Si and CdTe modules. Section 8.7 shows the plots for the other modules.
When comparing all plots it is seen that both the rainy and non-rainy PR's are distributed near normal. The poly-Si A module is an exemption to this *rule*. The PR distribution under non-rainy weather conditions is broad and the mean and mode values for PR are different (e.g. there is no clear bell shaped distribution). The majority of recorded non-rainy PR's furthermore are a lot lower than those of the other modules.
For the CIS module it is striking that although the distribution are near normal, like the other modules, the peaks of both the rainy and non-rainy PR's are lower than the others. The absolute PR's are therefore also lower. These observations give rise to the assumption that these specific modules are faulty and that their performance can't be used as a technology specific benchmark.
Figure 22 furthermore shows that the significant difference in distributions of the a-Si and CdTe modules. On most occasions these modules perform better under rainy weather conditions. The relatively high values for rainy PR measurements (> 100%) can again be explained by the delayed temperature drop which affects the temperature correction and thus PR.

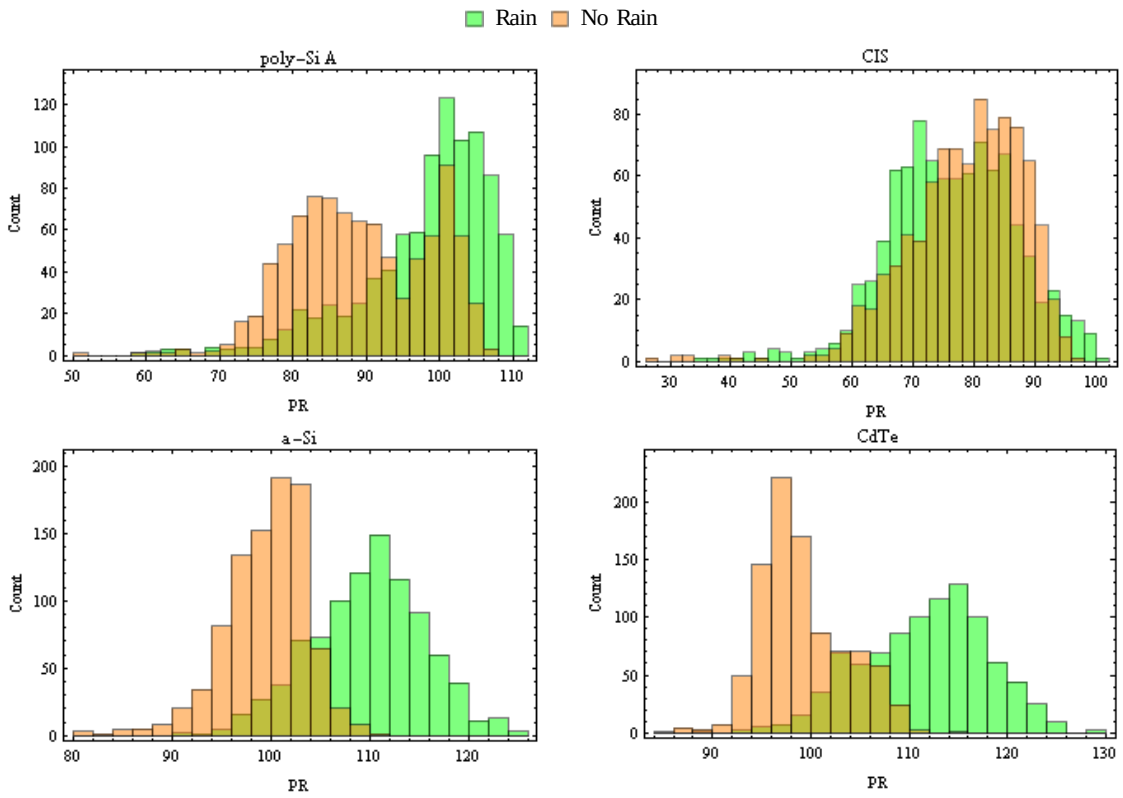

Figure 22 Distribution in PR during rainy and non-rainy time periods. The broad and non-normal distribution in PR values for the poly-Si A module indicate that performance of this module shouldn't be used to make a generalization for other modules of this type (there is probably something wrong with this module). The same holds for the CIS module which has a lot of low values in PR.

5 Discussion and recommendations

5.1 Quantification of the precipitation effect on the solar spectrum

Water absorbing solar radiation at near infrared wavelengths indicates that the severity of precipitation will have an effect on the spectral composition of downwelling irradiance; more rain will cause more long-wavelength photons to be absorbed, leaving relatively more short-wavelength photons to continue their path to the earth's surface which will result in an increase of APE. From the recorded data this intensity effect on the solar spectrum is however hard to determine.

In section 2.1.5 it has been indicated that as AM increases the amount of Rayleigh scattered short wavelength photons increases resulting in a decrease in APE. Therefore mean APE values around solar-noon will generally be higher than during sunrise and sunset. The solar geometry furthermore results in the AM changing throughout the year. If we look at the time periods shown in Figure 23 of section 8.2 and compare the AM during the period of high precipitation with that of low precipitation it is found that the latter has higher values (a combination of time of day and time of year effect). APE values are therefore presumed to be higher during the first time period. If then the intensity of precipitation were to have a positive effect on the APE a compounded effect would be expected an, the first time period would have a higher APE (i.e. both AM and the precipitation intensity would cause the APE to be higher). This is however not noticeable; both time periods show the same mean value for APE. A counterargument to this observation could be that the time periods pertain to different days and it could well be that other factors are therefore at play, which cause the mean APE to be similar (e.g. atmospheric conditions).

One way of determining the correlation between precipitation intensity and APE would be to bin measurements in which AM and climatic conditions are equal and perform a regression between the two parameters. Firstly, this would require a larger dataset than the one used for this study. Secondly, it would require the timestamp measurements to coincide. The APE and precipitation intensity measurements used in this study were not recorded during the same timestamps. This prevents a regression of these two parameters and makes it difficult to accurately determine the effect of the precipitation intensity on the spectral composition. Interpolation could be performed to align measurements by time, however, especially in fast changing conditions this would introduce significant uncertainty. The measurement timing should therefore be aligned if this presumable effect is to be investigated.

5.2 Accurate temperature measurements

Apart from APE and precipitation measurements not being recorded on the same timestamp the precipitation measurements and the module temperature measurements also do not coincide. Therefore a direct correlation between these two also cannot be estimated. Furthermore due to the temperature measurements being performed on the back of the module there could be a delay in the measured temperature drop. As suggested in section 4.2.2 this has probably resulted in inaccurate temperature corrections. It would be valuable to acquire insights into these temperature changes. A model could be developed which ascertains the temperature

development of a specific module under varying climatic conditions. To this end an IR camera could be used which measures temperatures at the front end of the module whilst the temperature sensors at the back also take measurements. Results from such a model could serve two purposes. Temperature correction factors could be derived which, when applied, yield more accurate estimations of PR. Secondly comparison of the results to temperature development calculations performed with the use of values for thermal conductivity could be used to identify any major module defects and be used as a quality assurance tool.

6 Conclusion

The lack in knowledge about PV performance under rainy weather conditions was the driver for this research which used results from a PV test facility located at the Utrecht University to determine the effects of precipitation on I_{SC}, V_{OC} and PR. The results show that, although there is discrepancy between technologies, with the exemption of the CIS module all investigated PV modules, operating under low irradiance levels, have a higher performance during rainy than under non-rainy weather conditions. Precipitation causes module temperatures to drop resulting in increased open circuit voltage. At low irradiance levels precipitation furthermore seems to shift the spectral irradiance more towards the blue resulting in short circuit current to increase for modules which have a higher spectral responsiveness in this region. The combined performance enhancement, given in terms of PR, showed that precipitation can increase performance by up to more than 12%. It should however be noted that part of this increase might be caused by measurement inaccuracies. Temperature corrections for instance are applied to account for losses in V_{OC} caused by measured T_{module} rising above STC T_{module}. Measured T_{module} at the back end is higher than that at the front end where incident photons excite electrons. Deviations from STC temperature are therefore too high resulting in temperature corrections being too high also. As a result presented temperature corrected PR values attribute too much difference between rainy and non-rainy PR's to a shift in spectral irradiance. Accounting for this still yields significantly higher PRs for a-Si and CdTe modules during rainy weather conditions.

As shares of renewable energy sources increase in the energy mix the intermittency of renewable power forms a daunting challenge. The insights into the performance under rainy weather conditions presented in this work could aid forecasters in determining projected power outputs by PV systems under sub-optimal weather conditions and strengthen the case for renewable power.

7 References

[1] Barlett J, Ciotti A, Davis R, Cullen J. *The spectral effects of clouds on solar irradiance*. Journal of Geophysical Research 1998; 103(13):31,017-31,031

[2] KNMI, http://www.knmi.nl/klimatologie/uurgegevens/selectie.cgi

[3] Ishii T, Otani K, Takashima T. *Effects of solar spectrum and module temperature on outdoor performance of photovoltaic modules in round-robin measurements in Japan*. Progress in Photovoltaics: Research and Applications 2011; 19: 141-148

[4] Ishii T, Otani K, Takashima T, Ikeda K. *Change in I-V characteristics of thin-film photovoltaic (PV) modules induced by light soaking and thermal annealing* effects. Progress in Photovoltaics: Research and Applications 2013

[5] Ishii T, Otani K, Takashima T, Xue Y. *Solar spectral influence on the performance of photovoltaic (PV) modules under fine weather and cloudy weather* conditions. Progress in Photovoltaics: Research and Applications 2013; 21: 481-489

[6] Nofuentes G, García-Domingo B, Muñoz J, Chenlo F. *Analysis of the dependence of the spectral factor of some PV technologies on the solar spectrum distribution*. Applied Energy 2014; 113: 302-309

[7] Cornaro C, Andreotti A. *Influence of Average Photon Energy index on solar irradiance characteristics and outdoor performance of photovoltaic modules*. Progress in Photovoltaics: Research and Applications 2013; 21: 996-1003

[8] Rahim R, Baharuddin, Mulyadi R. *Classification of daylight and radiation data into three sky conditions by cloud ratio and sunshine duration*. Energy and Buildings 2004; 36: 660-666

[9] Sutterlueti J, Ransome S, Kravets R, Schreier L. *Characterising PV modules under outdoor conditions: what's most important for energy* yield. 26th EU PVSEC, Hamburg, Germany 2011

[10] Usami A, Kawasaki N. *Modeling of solar spectral irradiance data from cloudless to overcast skies*. Japanese Journal of Applied Physics 2012; 51

[11] van Sark W.J.G.H.M., Louwen A, de Waal A, Elsinga B, Schropp R. E.I. *UPOT: The Utrecht photovoltaic outdoor test facility*. 27th EU PVSEC, Frankfurt, Germany 2012

[12] Honsberg C, Bowden S. *PVCDROM*, http://pveducation.org/pvcdrom

[13] Bird R.E., Riordan C. *Simple solar spectral model for direct and diffuse irradiance on horizontal and tilted planes at the earth's surface for cloudless atmospheres*. Journal of climate and applied meteorology 1986; 25: 87-97

[14] J. Twidell and T. Weir. *Renewable Energy Resources*. Taylor & Francis, Milton Park, Abingdon, 2nd edition, 2006.

[15] Emery, K. *Reference AM 1.5 spectra*, http://rredc.nrel.gov/solar/spectra/am1.5/

[16] ten Kate O.M., Personal communication, 2014-02-11

[17] Minemoto, T., Toda, M., Nagae, S., Gotoh, M., Nakajima, A., Yamamoto, K., . . . Hamakawa, Y.. *Effect of spectral irradiance distribution on the outdoor performance of amorphous Si/thin-film crystalline Si stacked photovoltaic modules*. Solar Energy Materials and Solar Cells 2007; 91: 120-122

[18] Williams, S., Betts, T., Helf, T., Gottschalg, R., Beyer, H., & Infield, D.. *Modeling long-term module performance based on realistic reporting conditions with consideration to spectral effects*. Proceedings of the Third World Conference on Photovoltaic Energy Conversion, Osaka, Japan 2003

[19] Muller R.S., Kamins T.I., Chan M. *Device electronics for integrated circuits*. John Wiley & Sons, New York, 3rd edition, 2003
[20] N. H. Reich, B. Mueller, A. Armbruster, van W. G. J. H. M. Sark, K. Kiefer, and C. Reise. *Performance ratio revisited: is pr > 90 % realistic?,* Progress in Photovoltaics: Research and Applications 2012; 20:717–726
[21] EKO Instruments, http://eko-eu.com
[22] Lufft GmbH, http://www.lufft.com/en/
[23] National Instruments, http://www.ni.com/labview/
[24] Wolfram Mathematica, http://www.wolfram.com/mathematica/
[25] Stein J. S., Reno M.J., Hansen C.W.. *The variability index: a new and novel metric for quantifying irradiance and PV output variability*. Sandia National Laboratories

8 Appendix

8.1 Temperature effect on V_{OC}

The negative effect of module temperature on V_{OC} is explained through the dependency of V_{OC} on the reverse saturation current I_0;

$$V_{OC} = \frac{kT}{q}\ln\left(\frac{I_{SC}}{I_0}\right) = \frac{kT}{q}[\ln(I_{SC}) - \ln(I_0)]$$

Equation 19

From Equation 19 it becomes clear that an increase in I_0 will result in a decrease in V_{OC}. I_0 is given by Equation 20;

$$I_0 = qA\left(\sqrt{\frac{D_p}{\tau_p}} * \frac{n_i^2}{N_D} + \sqrt{\frac{D_n}{\tau_n}} * \frac{n_i^2}{N_A}\right)$$

Equation 20

Where A stands for the surface area, D_p and D_n stand for the hole and electron diffusion coefficients, τ_p and τ_n stand for the excess carrier lifetimes, N_D and N_A represent the donor and acceptor atomic densities and n_i^2 resembles the intrinsic carrier concentration. Given that all parameters, with the exception of n_i^2 are of negligibly or no dependence on temperature, the equation for the reverse saturation current can be rewritten in the form of;

$$I_0 = constant_1 * n_i^2$$

Equation 21

The intrinsic carrier concentration is given by ;

$$n_i^2 = N_C * N_V * e^{-E_g/kT}$$

Equation 22

Where E_g is the bandgap and N_C and N_V are referred to as the effective densities of state in the conduction and valence band and are given by Equation 23 and Equation 24;

$$N_C = 2 * \left(\frac{2\pi m_e^* kT}{h^2}\right)^{3/2} = constant_2 * T^{3/2}$$

Equation 23

$$N_V = 2 * \left(\frac{2\pi m_h^* kT}{h^2}\right)^{3/2} = constant_3 * T^{3/2}$$

Equation 24

Here m_e^* and m_h^* are the effective masses of an electron in the conduction band and hole in the valence band respectively. Combining Equation 22, Equation 23 and Equation 24 yields;

$$n_i^2 = constant_2 * T^{3}/_2 * constant_3 * T^{3}/_2 * e^{-Eg/kT} = constant_4 * T^3 * e^{-E_g/kT}$$

Equation 25

Substitution of n_i^2 in Equation 21 with the outcome of Equation 25 yields;

$$I_0 = constant_5 * T^3 * e^{-Eg/kT}$$

Equation 26

Further substitution of the saturation current into the equation for V_{OC} yields;

$$V_{OC} = \frac{kT}{q}\left[\ln(I_{SC}) - \ln\left(constant_5 * T^3 * e^{-Eg/kT}\right)\right]$$
$$= \frac{kT}{q}\left[\ln(I_{SC}) - \ln(constant_5) - 3\ln(T) + \frac{E_g}{kT}\right]$$

Equation 27

From Equation 27 it becomes clear that an increase in temperature will result in a decrease in V_{OC} [12].

8.2 Time periods used in dataset

Rainy moments					Non-rainy moments				
Date	Start	End	Hours	Measurements	Date	Start	End	Hours	Measurements
4-26	9	18	9	129	5-2	9	13	4	114
4-29	9	12	3	54	5-29	15	18	3	50
5-11	9	13	4	96	6-1	9	13	4	77
5-16	9	18	9	230	6-10	9	11	2	40
5-20	15	18	3	78	6-30	10	12	2	31
5-21	14	18	4	71	7-5	9	10	1	28
6-21	10	14	4	57	7-11	9	12	3	59
6-23	10	12	2	31	9-7	9	13	4	75
6-28	9	12	3	28	9-20	9	11	2	40
9-14	13	16	3	56	9-22	9	12	3	53
10-11	9	18	9	36	9-24	9	12	3	56
11-4	11	13	2	61	10-12	9	11	2	34
					10-15	9	11	2	37
					10-18	9	13	4	63
					10-21	10	13	3	59
					11-1	9	13	4	79

Total measurements	**927**	**Total measurements**	**895**

8.3 Precipitation intensity effect

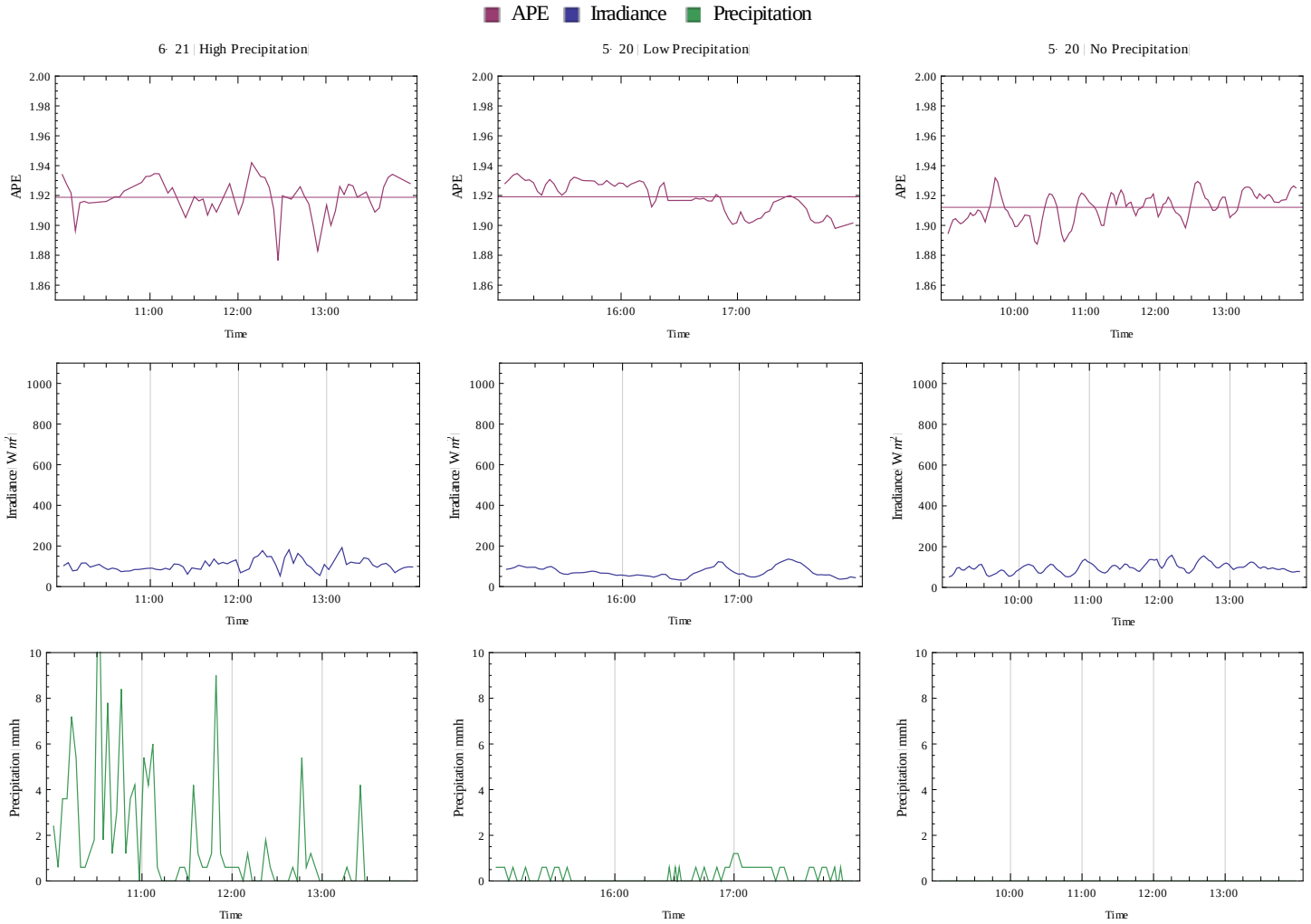

Figure 23 Comparison of three time periods used for identifying whether the intensity of precipitation affects I_{SC}. The top three plots indicate that the mean APE is fairly equal (solid horizontal lines). The middle plots give the H_{POA} and show that it remains constant throughout and equal across the three time periods. The bottom plots finally confirm that the precipitation intensity differs.

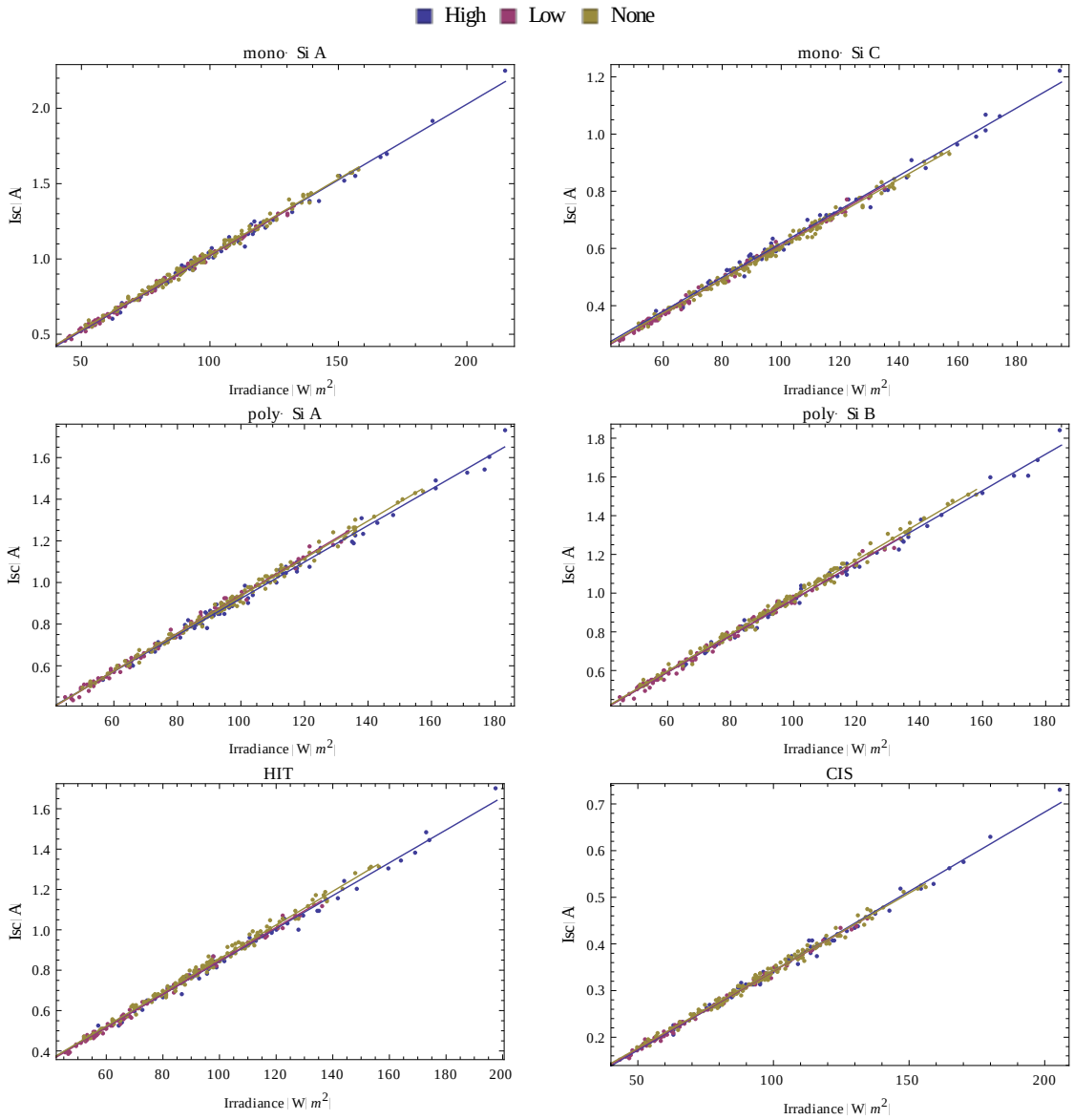

Figure 24 Temperature corrected values for I_{SC} set out against H_{POA} under equal levels of mean APE and three different levels of precipitation (remaining modules).

8.4 I_{SC} VS H_{POA}

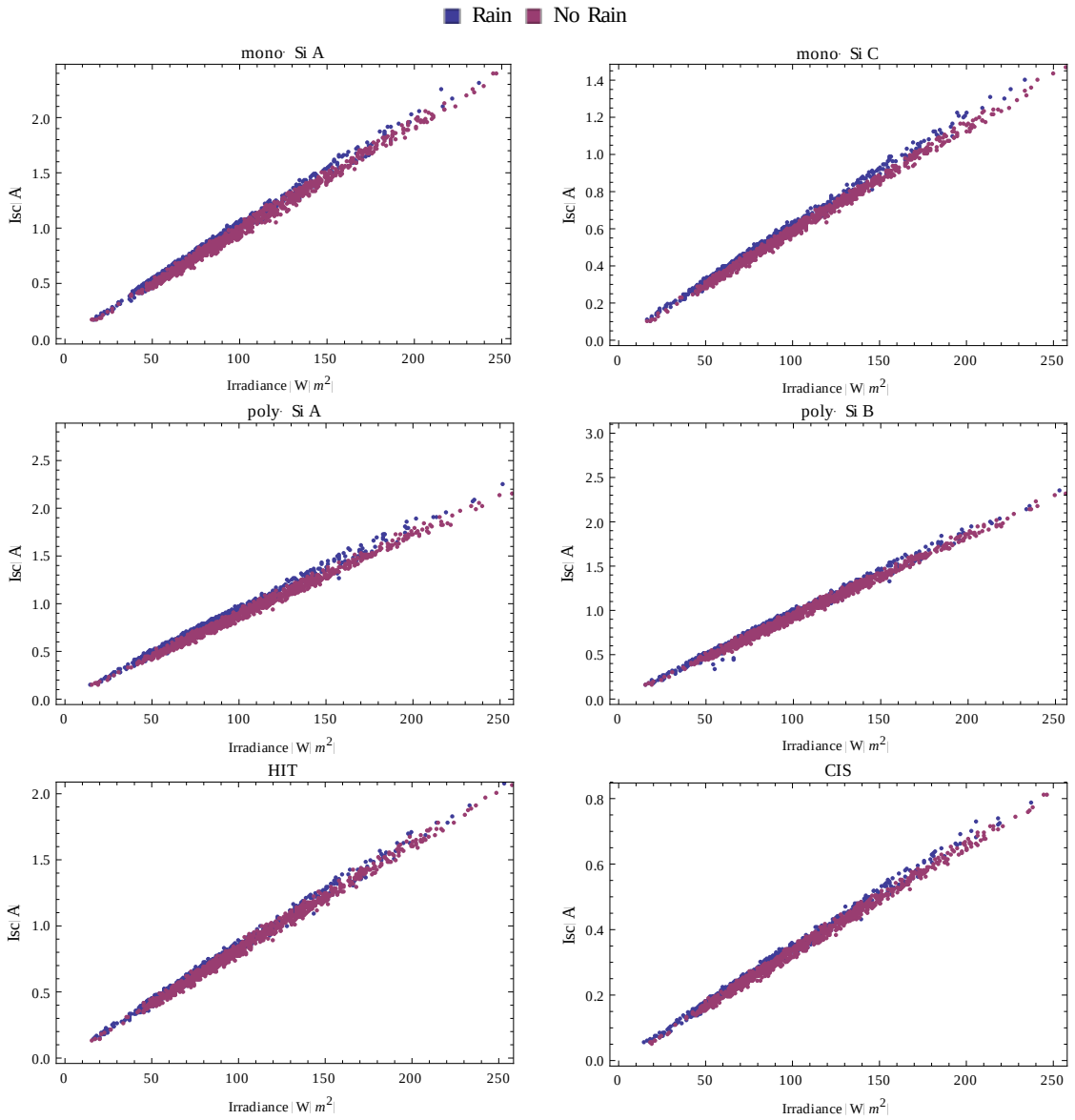

Figure 25 Temperature corrected values for I_{SC} set out against H_{POA} under rainy and non-rainy time periods (remaining modules).

8.5 V_{OC} VS H_{POA} non-temperature corrected

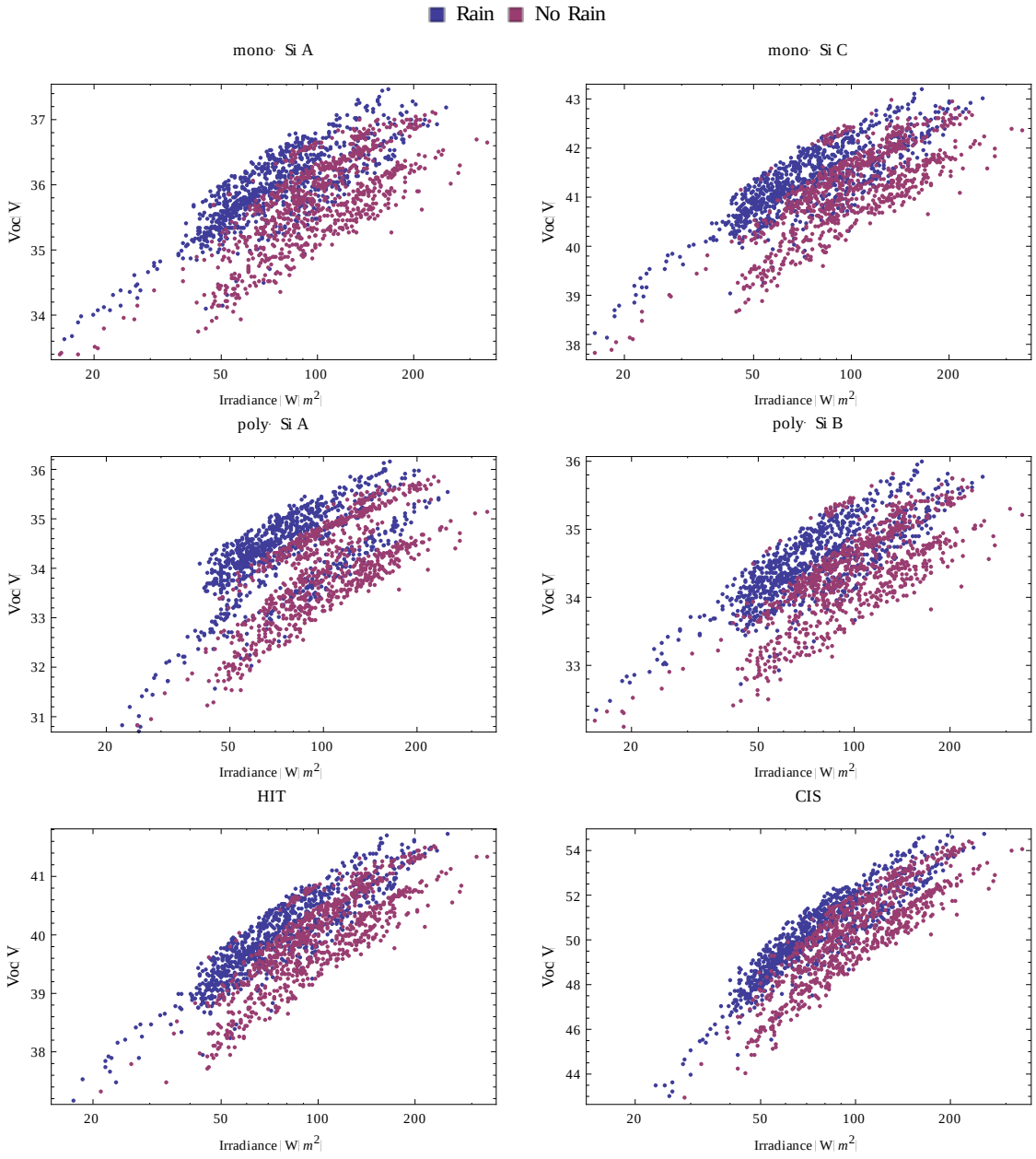

Figure 26 Non-temperature corrected values for V_{OC} (logarithmic scale) set out against H_{POA} under rainy and non-rainy time periods (remaining modules).

8.6 V_{OC} VS H_{POA} temperature corrected

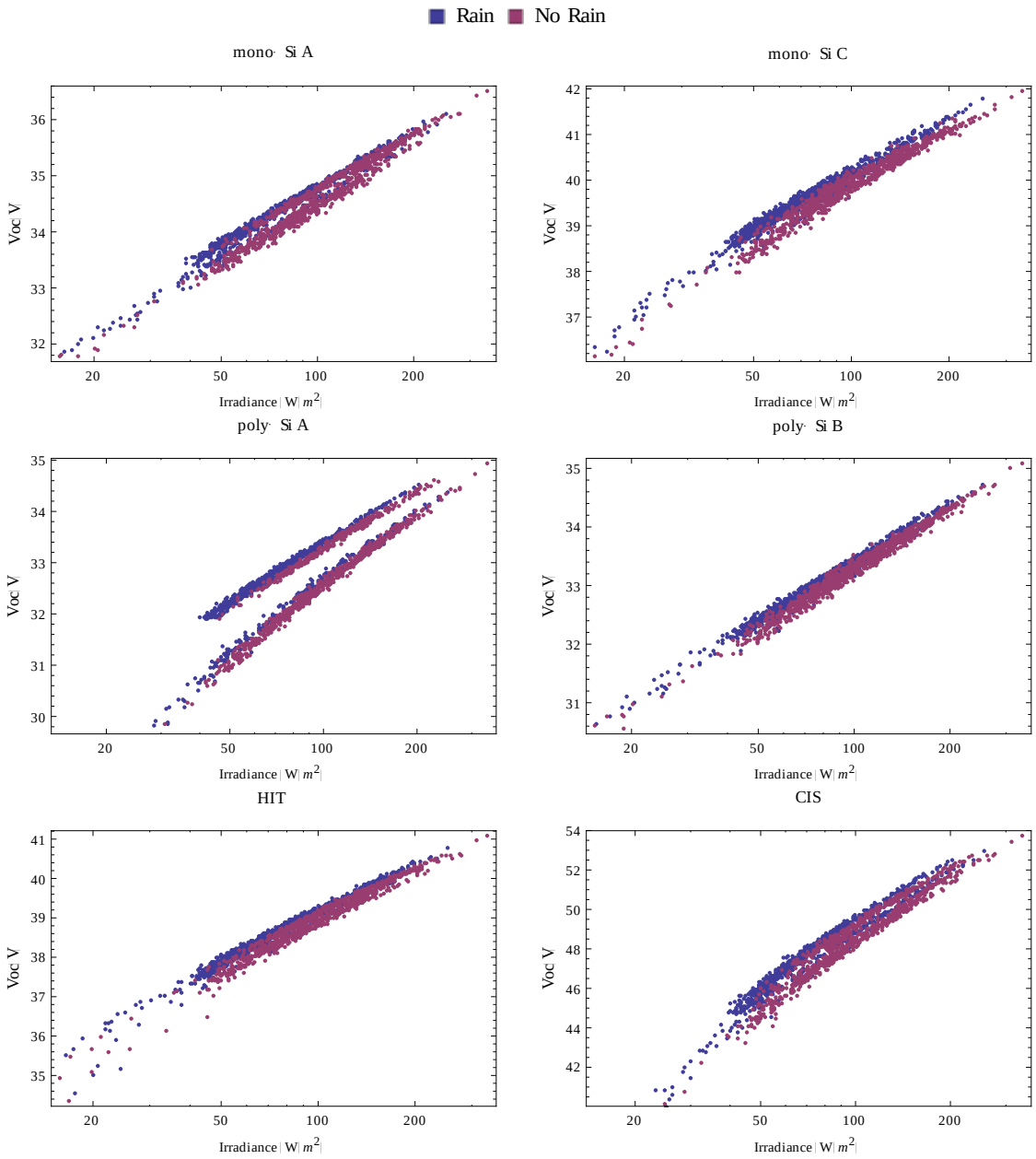

Figure 27 Temperature corrected values for V_{OC} (logarithmic scale) set out against H_{POA} under rainy and non-rainy time periods (remaining modules).

8.7 PR distributions

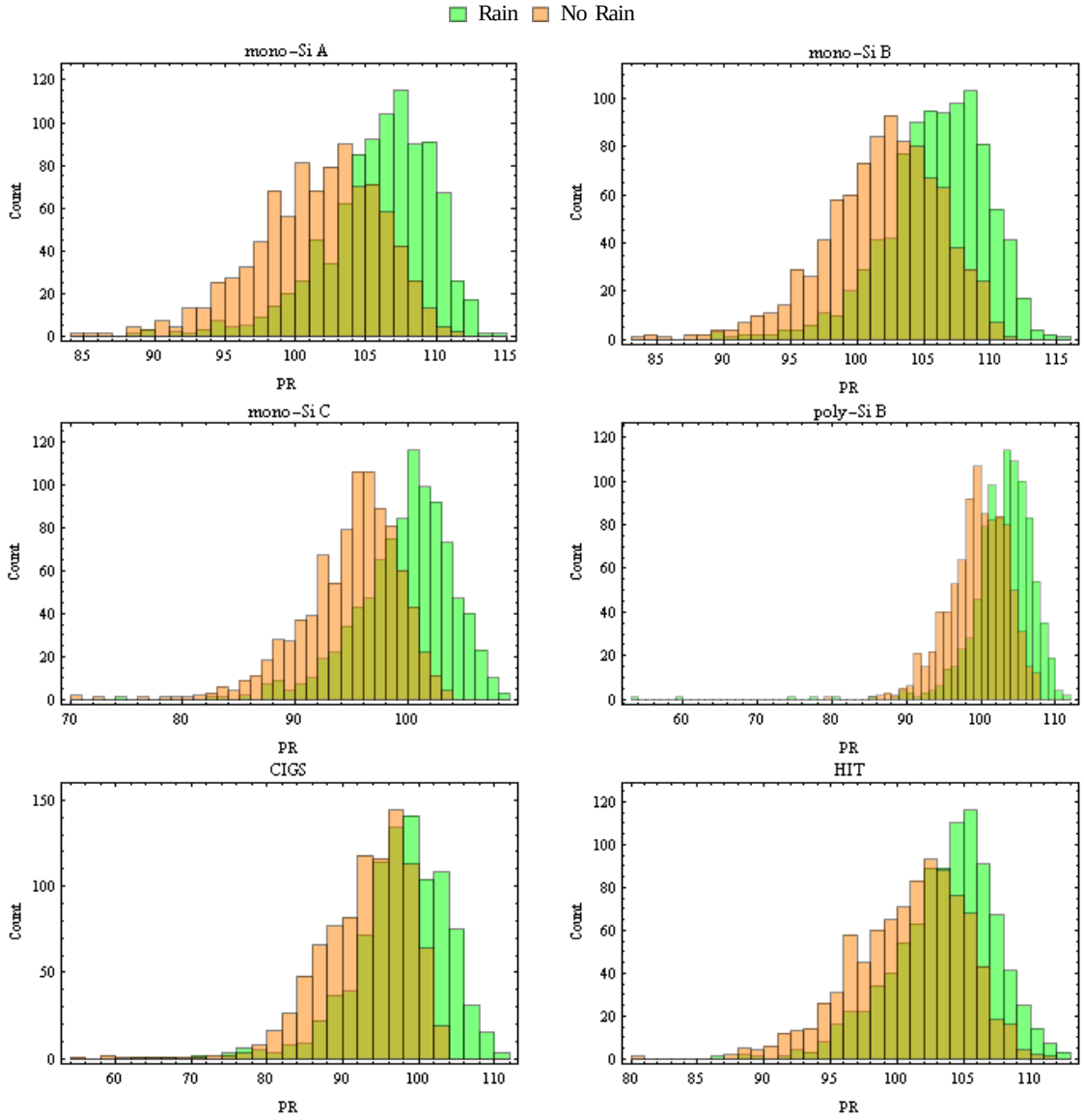

Figure 28 Distribution in PR during rainy and non-rainy time periods (remaining modules).